Q. J. R. Meteorol. Soc. (1993), **119**, pp. 975–1001 551.584.3:551.551.8:551.509.313.31:551.510.522(781)

Comparison between the land surface response of the ECMWF model and the FIFE-1987 data

By ALAN K. BETTS* and JOHN H. BALL
Atmospheric Research, Pittsford, USA
and
ANTON C. M. BELJAARS
European Centre for Medium-range Weather Forecasts, Reading, UK

(Received 6 October 1992; revised 22 January 1993)

SUMMARY

An averaged time series for the surface data for the 15 × 15 km FIFE site was prepared for the summer of 1987. Comparisons with 48-hour forecasts from the ECMWF model for extended periods in July, August and October 1987 identified model errors in the incoming short-wave radiation in clear skies, the ground heat flux, the formulation of surface evaporation, the soil-moisture model, and the entrainment at boundary-layer top.

The model clear-sky short-wave flux is too high at the surface by 5–10%. The ground heat flux is too large by a factor of 2 to 3 because of the large thermal capacity of the first soil layer (which is 7 cm thick), and a time truncation error. The surface evaporation was near zero in October 1987, rather than of order 70 W m^{-2} at noon. The surface evaporation falls too rapidly after rainfall, with a time-scale of a few days rather than the 7–10 days (or more) of the observations. On time-scales of more than a few days the specified 'climate layer' soil moisture, rather than the storage of precipitation, has a large control on the evapotranspiration. The boundary-layer-top entrainment is too low. This results in a moist bias in the boundary-layer mixing ratio of order 2 g Kg^{-1} in forecasts from an experimental analysis with nearly realistic surface fluxes; this because there is insufficient downward mixing of dry air.

1. INTRODUCTION

During 1987 an extensive series of surface data was collected (Sellers *et al.* 1988) over the Konza prairie in Kansas during the First ISLSCP (International Satellite Land-Surface Climatology Project) Field Experiment (FIFE). These data were reduced to a single mean time series (Betts and Ball 1992). This time series was compared with the time series at the closest grid point from short-term forecasts (48 hour), using the European Centre for Medium-range Weather Forecasts (ECMWF) global model, to identify possible errors in the model. We shall present averages for similar days in different seasons to show how this surface time series can be used to identify systematic errors in the ECMWF (abbreviated as EC hereafter) model. It might be thought remarkable that data from the 15 × 15 km domain of FIFE can readily detect systematic errors in a complex global model with a horizontal resolution of order 100 km. However, the accuracy of the forecast model over the dense US network, the representivity of the FIFE surface data in 1987 (after editing and averaging), and the existence of a long enough time series to select weather regimes (such as sunny days in different seasons) makes this relatively straightforward. Often errors at the one grid point (of FIFE) are representative of continental-scale errors, since they represent systematic errors in the model formulation. The variation in the EC model is smooth over this region of Kansas, and if we had chosen an adjacent grid point in the model, we would have reached similar conclusions about the model errors. We were able to identify apparent errors in the incoming short-wave radiation in clear skies, in the ground heat flux, in the formulation of the surface evaporation and the soil model, and in the boundary-layer-top entrainment.

Global models are initialized using synoptic data, most of which is at 12-hour intervals. Less use is made of the more frequent surface data, so that the surface diurnal cycle in the model is dominated by the model formulation. The FIFE data at 30-minute intervals can thus identify systematic errors in the model simulation of the diurnal cycle

* Corresponding author: Atmospheric Research, RR No. 3, Box 3125, Pittsford, VT 05763, USA.

over land, both at the surface and in the boundary layer (BL). By an iterative process of revising parts of the model, and again comparing with this and other data, we hope to improve the global forecast model steadily, and in particular to reduce the biases in the model climate over land, and in the model representation of the hydrologic cycle over land. Data from observational research programs provide a valuable framework for testing model parametrizations. Improved parametrizations for land-surface processes are needed in both forecast and climate models (Sellers *et al.* 1986; ECMWF 1988). Forecasting surface temperature and humidity depends on the accuracy of the land-surface and BL parametrizations. Routine assimilation of global data by forecast models also provides global analyses for climate research. Even the analysis of soil moisture may be possible on the basis of near-surface routine data (Mahfouf 1991), but it relies critically on the accuracy of the soil-moisture model as well as the boundary-layer parametrization. In addition, forecast models such as the EC model are also used at lower resolution for climate modelling, so the study of their systematic errors is valuable. This study shows the benefit of closer integration between field experiments and global models.

2. Data used

We used several sets of FIFE surface data. The PAM (Portable Automated Mesonet) station time-series data (30-minute averages at 10 stations) consisted of wind at 5.4 m, temperature and humidity at 2 m, together with a radiometric measure of the ground surface temperature, ground temperatures at 10 and 50 cm below the surface, incoming and reflected short-wave radiation, net radiation and incoming long-wave radiation, and rainfall. A data set of the mean surface sensible- (SH) and latent-heat (LH) fluxes and ground heat fluxes was also prepared: this was an average over 13 selected surface-flux stations, which made measurements using both eddy correlation and Bowen-ratio methods. These flux stations also measure all four radiation components and net radiation. A set of digitized photos from a whole-sky camera gave a measure of the fractional cloud cover. Gravimetric soil-moisture measurements for two subsurface layers (0–5 and 5–10 cm) were also reduced to a site average.

The raw data were filtered and screened by eye to remove bad values, and averaged to a single mean time series for the FIFE site. The PAM data from 26 May to 16 October 1987 were processed (from the first day of the First Intensive Field Campaign (IFC-1) to the last day of IFC-4). The averaged flux-station data are only available for the four IFCs of FIFE-1987, although some days of single-station data during a dry period in July will also be used. The raw data are available from the FIFE Information System (FIS). These reduced data sets, which are available on diskette from the authors (Betts and Ball 1992), are discussed in more detail in the appendix.

For the studies of the vertical structure of the BL, we used radiosonde data. Sondes were launched at roughly 90 min intervals on most sunny days. We determined a BL depth from the top of the nearly well-mixed layer: this could be determined to typically ±5 mb. The individual BL profiles were then scaled in pressure using this BL depth and interpolated to scaled pressure levels. Sets of sondes for selected days could then be averaged (see section 4(c)), while preserving the vertical structure within the BL, following the method of Betts (1976).

3. The ECMWF model

A T-106 L-19 cycle 39 version of the EC model was rerun for 48 hours from the 12 GMT analyses for three blocks of days: 1–18 July, 5–21 August and 5–13 October 1987.

For October, when conditions were rather dry, only the 1987 operational analyses (with cycle 29 of the model) were available. For July and August a T-106 L-19 experimental reanalysis of the data was also available using cycle 39 of the model. (This is the model that became operational in September 1991 with T-213 L-31 resolution and semi-Lagrangian advection.) This included a change in the ground water runoff, which appeared to have led to significant increases in the soil moisture, in comparison with the original 1987 analysis. However, after analysing the forecasts from this reanalysis, we discovered that the increases in soil moisture were due instead to an error in the specification of the subsurface climate fields (see later). We shall show results from both these analyses, since they illustrate different errors in the model. A post-analysis program was used to archive subsurface, surface and BL data and fluxes at the model grid point (38.69°N 96.75°W) closest to the FIFE site (centred at 39.05°N, 96.53°W).

The EC model used has 19 levels with three to six layers in the BL. The levels are defined in hybrid coordinates (Simmons and Strüfing 1981); the approximate heights above the surface of the lowest six levels are 33, 150, 390, 800, 1400 and 2100 m. The land-surface scheme has prognostic variables for temperature and moisture for the surface layer (7 cm thick) and a deep layer (42 cm thick) to represent time-scales of 24 hours and 10 days respectively. In addition a skin reservoir is provided to represent a wet film on vegetation after precipitation. The subsurface boundary condition is specified using a climate layer (also 42 cm thick) with fixed temperature and soil moisture. The deep climate fields, which are taken from Mintz and Serafini (1989), are fixed for each month in the operational analysis. However, the experimental reanalysis, which was run for July and August 1987, started from 30 June; by mistake it retained the June subsurface climate fields, which are cooler and moister than those for July and August. This had a considerable effect on the forecasts run from this reanalysis, since diffusion of soil moisture from the moist climate layer enhances the surface evaporation. The mistake was, however, fortunate because the observed deep-soil moisture in FIFE is in fact closer to this experimental analysis than to those specified in the operational analysis. The model parametrization of evaporation consists of a wet surface part (including snow) with zero surface resistance, a bare-soil fraction with a relative humidity condition at the surface, and a vegetation fraction with a stomatal resistance. The relative humidity condition for bare soil depends on the soil moisture in the surface layer. The vegetation fraction is 85% at this grid point. The unstressed stomatal resistance is 25 s m^{-1}. This is then divided by a 'moisture availability in the root zone', which falls from one to zero as the mean soil moisture (a simple average of soil moisture in the 7 cm surface layer and the 42 cm deep layer) falls from 60% to 30% of the soil field capacity. The water extraction by the roots is weighted by the soil-moisture content; in the case of a uniform soil-moisture profile, equal amounts of water are extracted from the two layers, resulting initially in a six times faster decrease in the surface layer than in the deep layer. The land-surface scheme is described in Blondin (1991). Details of the BL scheme are given in Louis (1979) and Louis *et al.* (1982).

4. Comparison between cycle 39 and FIFE data

In this section we show some comparisons between the FIFE data and a recent version of the EC model (cycle 38, plus the physics updates from cycle 39; which we shall refer to here as cycle 39).

(*a*) *October comparison*

For the first comparison we take IFC-4 in October, when conditions were dry after the surface vegetation had largely died; the comparison is simplified by low cloud cover and low surface evaporation. The diurnal cycle on individual days can be influenced by advective processes. To give some indication of systematic differences in the diurnal cycle between the model forecasts and the data, we averaged seven days in October, which were predominately sunny in both data and model, to give an October 'clear-sky diurnal climate' comparison. We ran 48-hour forecasts from each 12 GMT operational analysis, from 5 to 13 October. We then averaged over the seven verifying 24-hour periods, which comprised the four days between 12 GMT on 6 October and 12 GMT on 10 October and the three days between 12 GMT on 11 October and 12 GMT on 14 October. Because we have 48-hour forecasts we can look at the corresponding verifying 7-day average for both the first and second days of the model forecast (referred to as Day 1 and Day 2) to give some indication of the model drift in the first 48 hours of the forecast. Note that because they have the same verifying dates, the end of Day 1 does not correspond to the beginning of Day 2 in the figures.

Figure 1 compares the diurnal cycle of the incoming solar radiation with the reflected solar radiation from two data sources (the 'PAM' average from the surface PAM stations, and the 'FLUX' average from the surface-flux stations) with this 7-day composite EC forecast. The x-axis is 24 hours starting from 1200 GMT. Local solar noon is about 1820 GMT, or 6.3 hours on Fig. 1. The surface-station averages differ by about 20 W m^{-2}, typical of the accuracy of this measurement. We consider the FLUX data (solid lines) to be the best radiation measurements (see appendix). These were days with little cloud in both model and observations, and the EC model incoming solar flux is higher than the data. The differences between Day 1 and Day 2 of the forecast are small. On individual

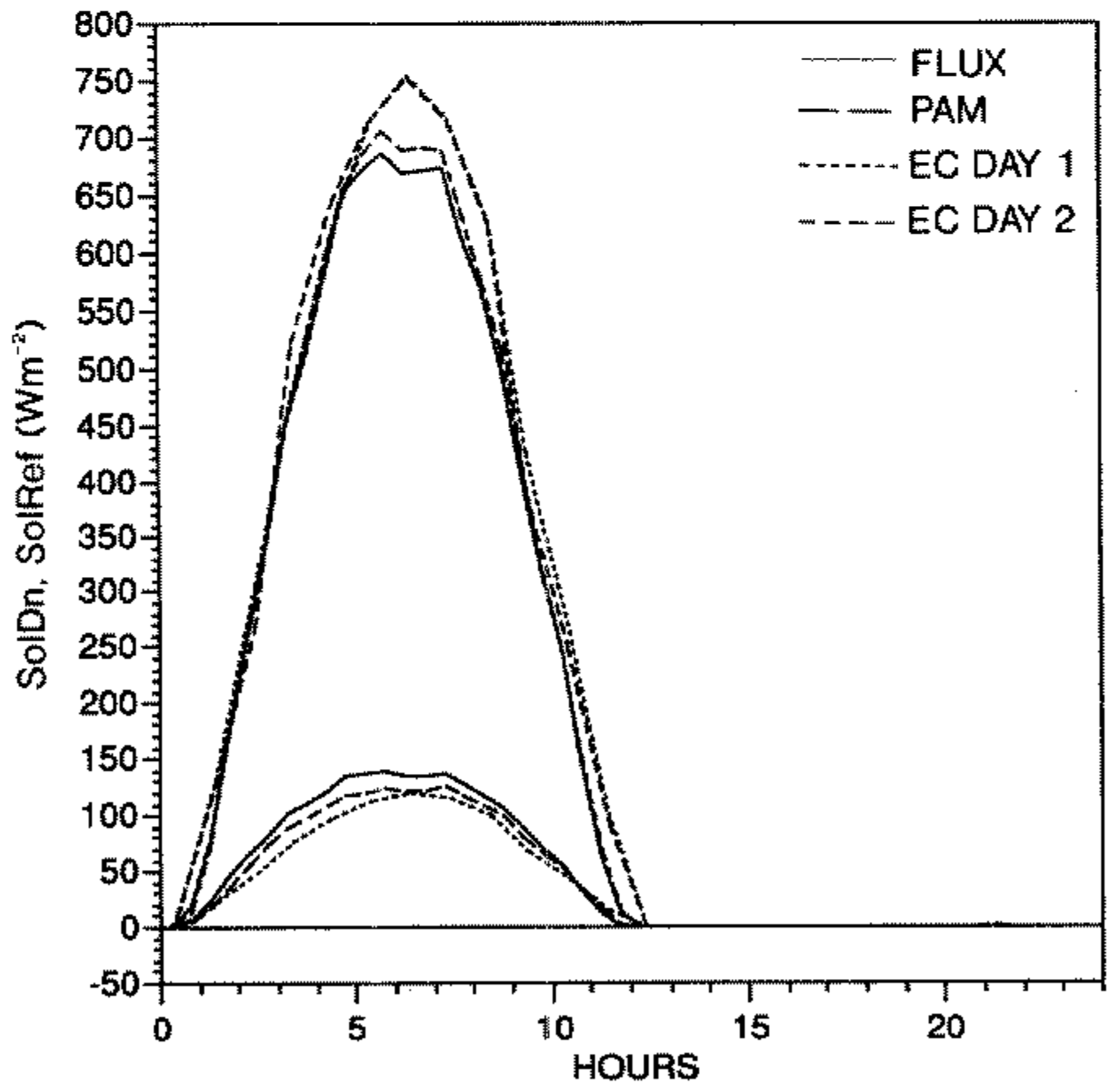

Figure 1. Incoming and reflected solar radiation (SolDn and SolRef respectively) from the PAM average from the surface PAM stations, and the FLUX average from the surface-flux stations for a 24-hour period starting at 1200 GMT for 7-day October 1987 average compared with the average of the forecasts from the ECMWF model with the same verification dates.

days, such as 7 October (not shown), when the EC model has very little cloud at this grid point, the model incoming solar flux is about 80–100 $W m^{-2}$ (over 10%) higher than the data. This is surprising, as it suggests that the clear-sky solar flux in the model is too high. Comparisons with the data on other selected clear days during the summer, where there is little or no cloud in the model, confirm this bias. In averages, cloudiness in the model tends to reduce this bias. The model has a fixed albedo at this grid point of 0.16, while the two sets of surface data have (near solar noon) slightly higher values: 0.18 for the PAM data and 0.21 for the FLUX data. Figure 2 shows the net radiation; the difference between model and data has become larger, partly because of these albedo differences. The data are direct measurements with well calibrated net radiometers. (They were well calibrated, since net radiation is critical in the Bowen-ratio method for finding the surface fluxes.) These independent net radiation measurements support our conclusion that the incoming solar radiation is too high in the model. Note that at night the net outgoing radiative flux is much higher in the model: this is because the ground surface layer is too warm, and is cooling by long-wave radiation. A small contribution ($\approx$10 $W m^{-2}$) to this difference may come from underprediction of the downward long-wave radiation in the model. The measurements of downward long-wave radiation (not shown) are probably less reliable though than the net radiation measurements.

We show both radiation data averages to give some indication of the uncertainty of the data. However the 'FLUX' radiation averages, which show lower incoming solar radiation and a higher albedo, are internally more self consistent: that is the net radiation measured directly most closely balances the sum of the four components measured and averaged separately (see appendix). Although this comparison is compromised by the fact that not all components were measured at all sites, the internal self-consistency gives us more confidence in the flux radiation data.

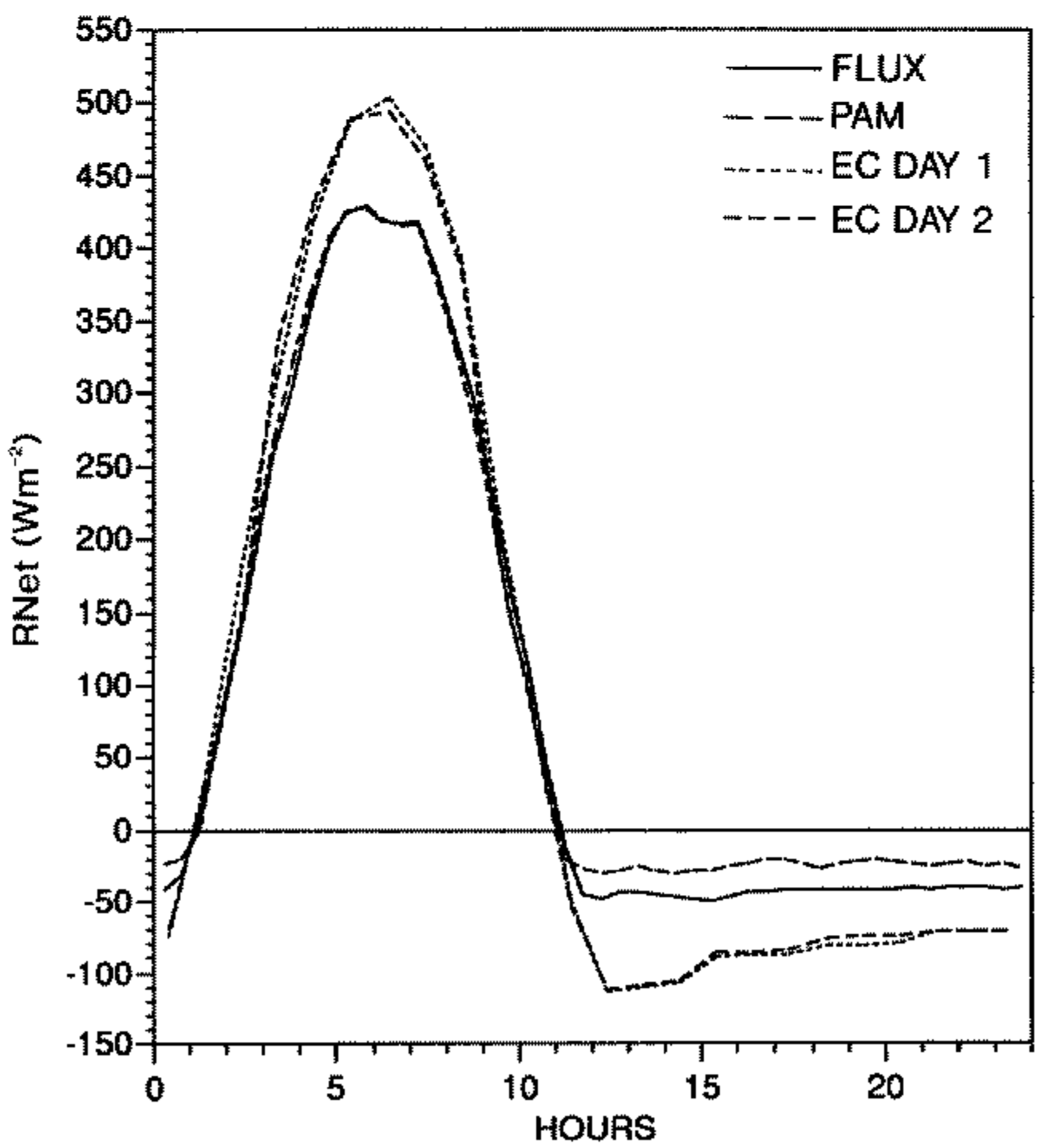

Figure 2. As Fig. 1 but for net radiation (RNet).

Figure 3 shows the SH and LH fluxes. We have kept the sign convention of the FIFE archive in which SH, LH and the ground flux (see Fig. 4) are negative away from the surface. The day-time model fluxes are biased. The model soil is so dry (below 30% of the soil field capacity) that there is nearly zero evaporation in the model, whereas the data show LH $\approx -70\,\mathrm{W\,m^{-2}}$ at local noon. Therefore, as expected, the model SH flux is significantly larger than the data, but unexpectedly there is a phase-lag of order two hours between data and model. Figure 4 shows the reason: the large ground heat flux in the model. The first subsurface layer in the EC model is 7 cm thick. As this layer initially warms after sunrise, the ground heat flux in the model is much larger than the data, reaching a peak of order $200\,\mathrm{W\,m^{-2}}$. Closer investigation shows that part of the ground-heat-flux error is due to a time-truncation problem, although the thermal inertia of the 7 cm thick surface layer is the main reason. The time-truncation problem is related to the process splitting between the BL scheme and the land-surface scheme. In a single time step the BL profiles are integrated forward with an implicit scheme, keeping a constant temperature at the surface. The resulting fluxes are then used for the corresponding time step with the land-surface scheme. Consequently, when the temperature is rising steeply in the morning, the surface temperature as seen by the BL scheme lags, and is too low. Therefore the SH and LH fluxes are also too low, and the residual of the surface energy budget shows up as a time-truncation error in the ground heat flux, giving the sharp morning peaks in Fig. 4 (see Beljaars (1991) for a discussion of the numerics of the parametrized part of the equations).

Figure 5 compares the diurnal response of the 2 m air temperature. The 2 m temperature in the model is computed as part of the post-processing. It is interpolated between the surface and the lowest model level, using a profile that is consistent with the parametrization of the surface layer (see Geleyn (1988) for details). We see that the model is systematically warmer, and has a smaller temperature range between sunrise and afternoon temperature maximum. The fall of the model temperature after sunset is slower than the data: this is again related to the slow thermal response of the ground temperature. The morning temperature minimum in the model is too high, and the difference from the data increases from Day 1 to 2 of the forecast. (Recall that these are averages for the same verifying dates, but the Day 2 forecasts start from analyses which are 24 hours earlier.)

Figure 6 compares the 2 m air temperature with the surface temperature (TSfcK: a radiometric skin temperature for the data, and that of the model 7 cm ground layer, which is the only 'surface' temperature in this model cycle). The temperature difference during the day-time heating cycle between surface and 2 m becomes larger in the data than in the model. We have analysed the model coupling between the surface and the 2 m air temperature, using an experimental surface model (Beljaars and Betts 1992). The small ground–air temperature difference is related to the fact that the model has the same roughness length for heat and momentum, while the analysis of the data (Betts and Beljaars, personal communication), as well as earlier studies (Garratt and Hicks 1973; Garratt 1978), suggests that the roughness length for heat is at least an order of magnitude less than that for momentum. The large differences in surface temperature at night are mostly responsible for the differences in the net radiation in Fig. 2.

These different characteristics of the model are significant. The surface temperature and the air temperature at 2 m are closely coupled in the model. During this 24-hour average of seven sunny days, these model temperatures rise about 2 K, whereas for the observations the rise is nearer 1 K. The net heat flux into the ground in the model is about $10\,\mathrm{W\,m^{-2}}$ (averaged over 24 hours), whereas the observations show (more realistically) an average 24-hour ground flux *upward* of $3\,\mathrm{W\,m^{-2}}$; that is, the ground has

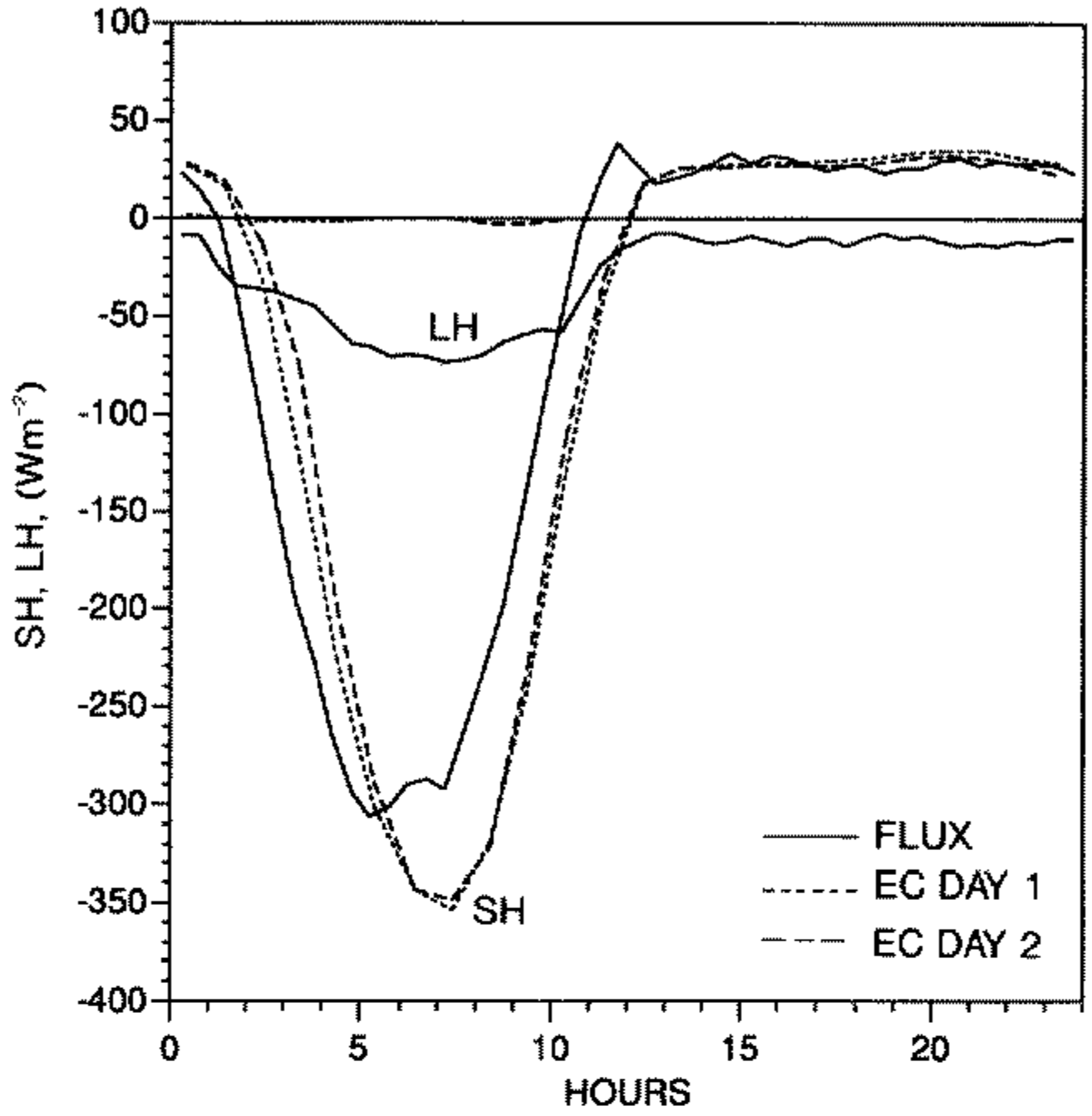

Figure 3. As Fig. 2 but for surface sensible- (SH) and latent-heat (LH) flux from FLUX data and the ECMWF model.

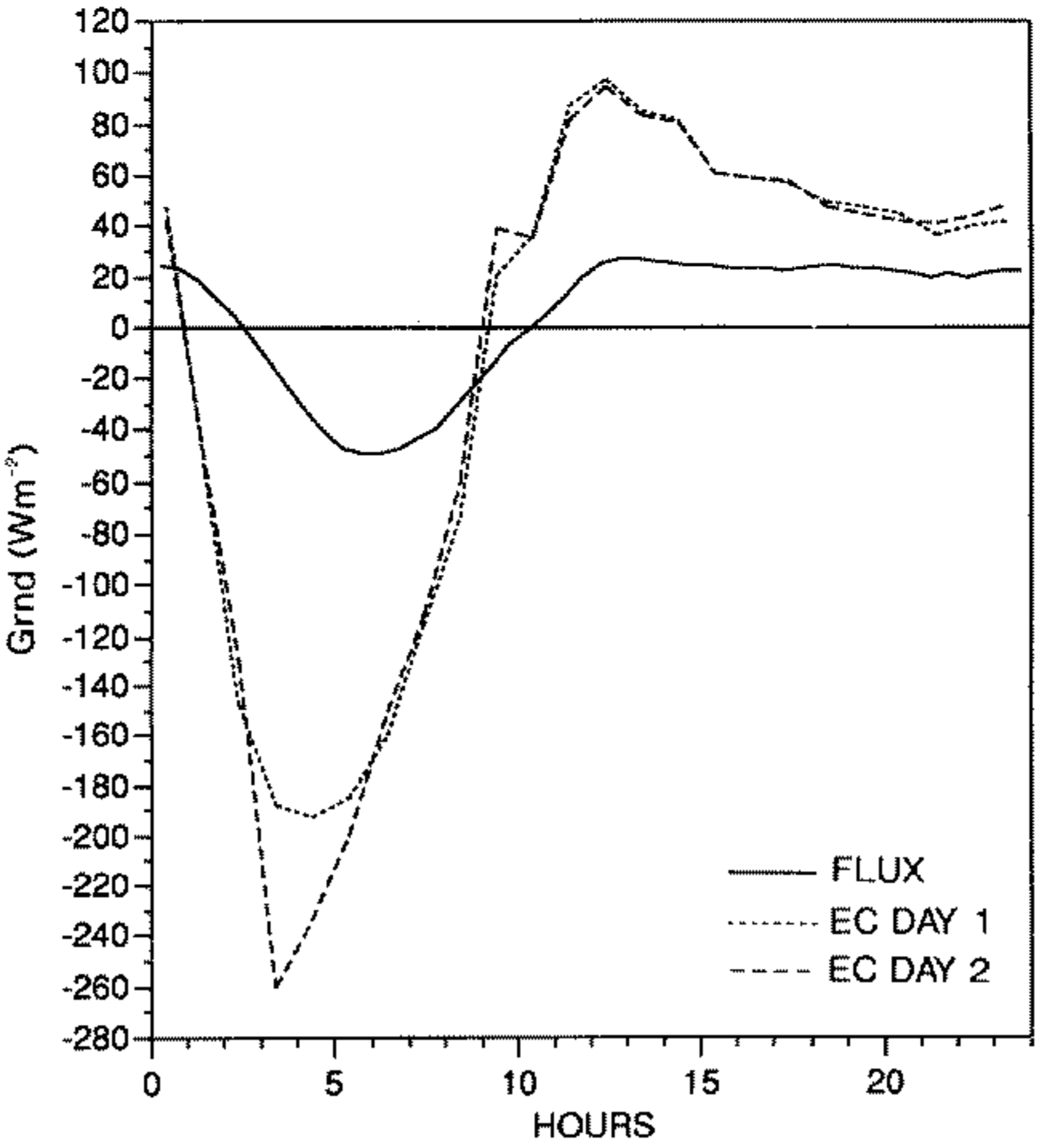

Figure 4. As Fig. 3 but for ground heat flux (Grnd).

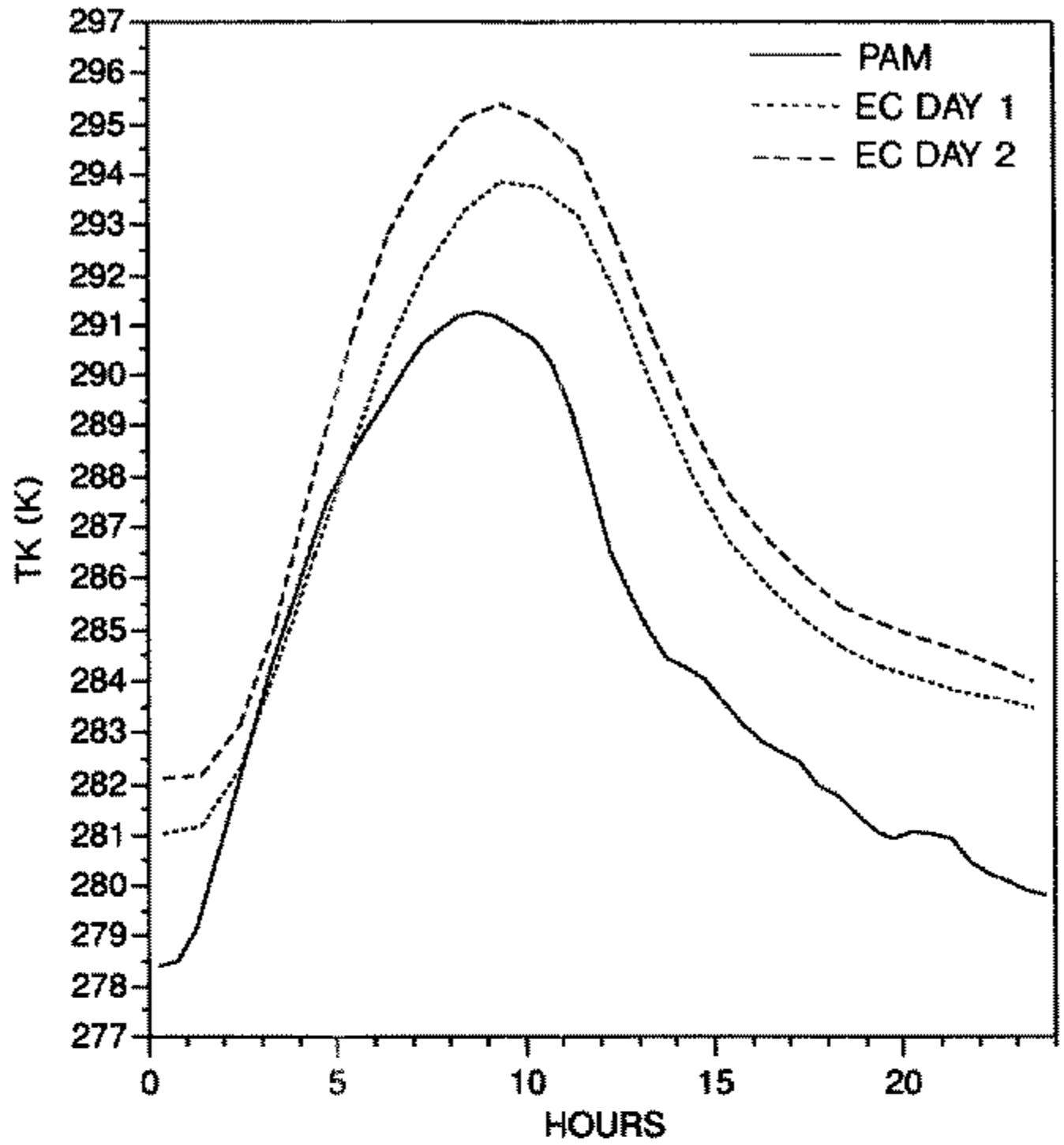

Figure 5. As Fig. 2 but for PAM 2 m air temperature (TK) and ECMWF forecast.

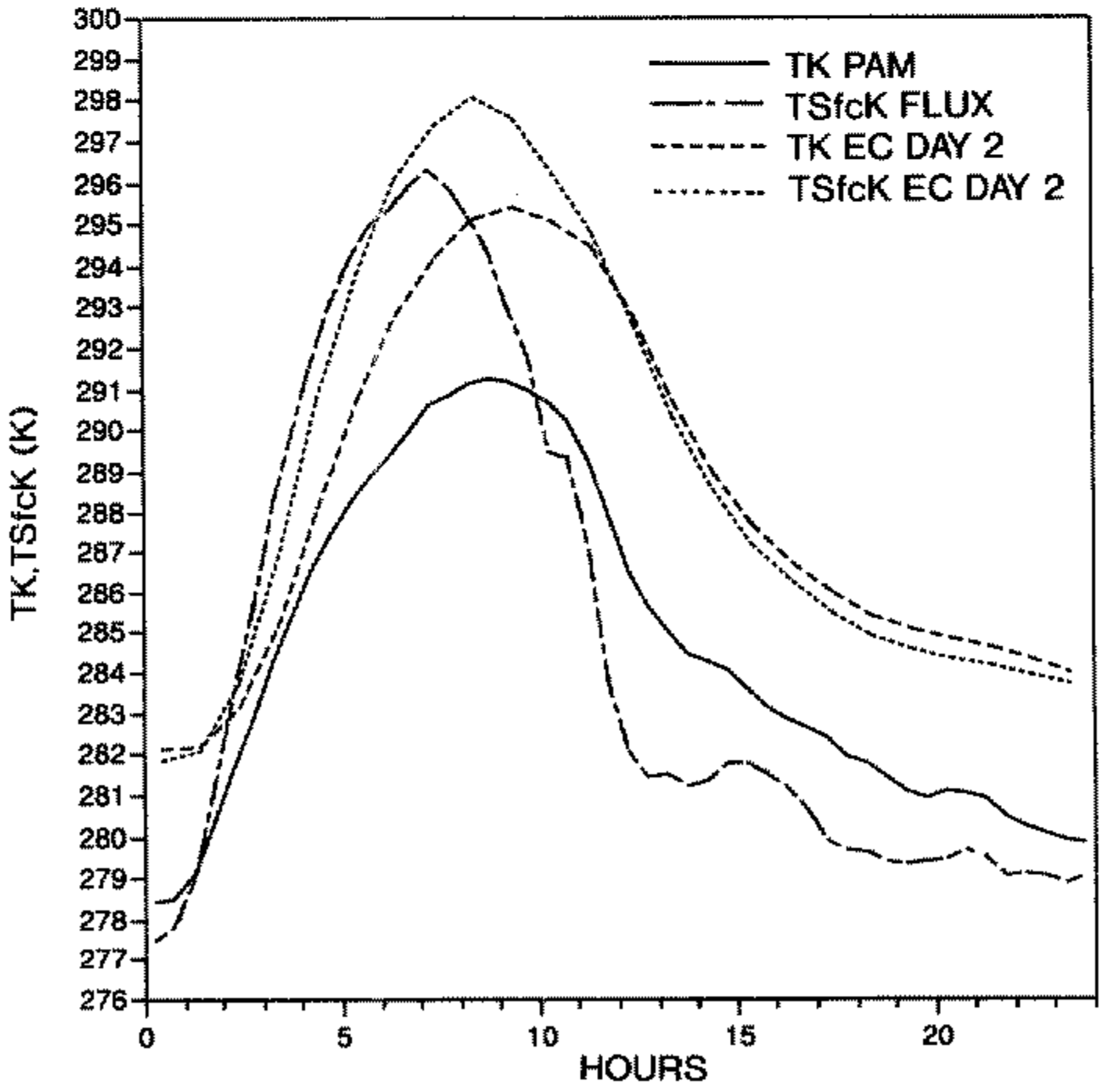

Figure 6. As Fig. 5 but for surface temperature (TSfcK) and 2 m air temperature (TK).

started to cool in October. The deep-soil temperature in the data is 290 K (at 50 cm); clearly it is conduction from the deep layers which are warming the surface on these sunny days, despite a net ground-flux upward. The deep 'climate' temperature in the model (below 49 cm) is similar; it is fixed at 289.5 K in October.

Figure 7 shows the trend of mixing ratio, q, for the data at 2 m, and the model value at the lowest model level, level 19 (roughly 33 m). (The model's interpolated 2 m value of q is not available as a post-processed product.) In the data, q has a small trend but the model dries rapidly in the first 24 hours and then stays dry. This is presumably because there is no surface evaporation.

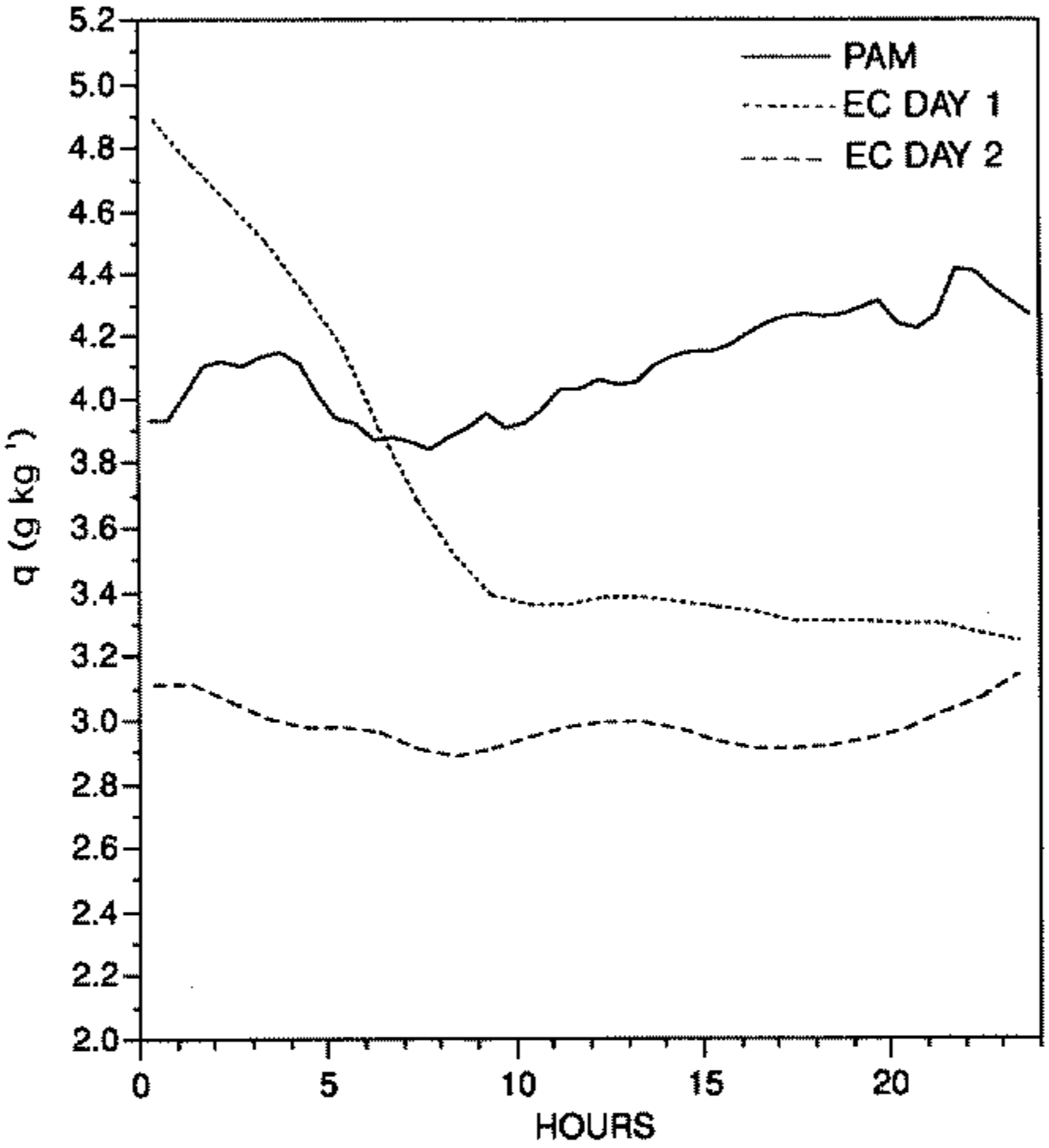

Figure 7. As Fig. 5 but for PAM 2 m mixing ratio (q) and ECMWF forecast, level 19 (33 m).

This October average shows a consistent picture, reflecting five systematic errors in the model.

(1) The incoming short-wave radiation is too high in clear-sky conditions, perhaps by as much as 10%. The fixed model albedo is lower than the data in October (this difference is less in August, see later), but this may be a unique to this grid point.

(2) The ground-surface model, which has a 7 cm thick first surface layer, is too slow to respond to the net radiation after sunrise, and cools too slowly at night. Since this layer must warm before the SH transfer to the atmosphere can become upward, the model needs a very large downward ground heat flux after sunrise, as large as 200 W m^{-2}. (The error is amplified by a time-truncation problem in the model.) This introduces a day-time phase lag into the upward SH flux, and appears also to result in a net heat flux into the ground, even as late in the year as October.

(3) The difference between surface temperature and air temperature is too small in the model. This is associated in part with having the same roughness lengths for heat and momentum in the model.

(4) The model LH flux is near zero in October. This results from ground-moisture values below the model threshold for evaporation (set at 30% of the soil field capacity). These are kept low by the soil moisture specified in the climate layer for October.

(5) The model BL dries out as a result of having no surface LH flux.

This drift of the model BL towards higher temperature and lower q is summarized on a (θ-q) plot in Fig. 8 (θ being the potential temperature). This shows the day-time hourly averaged values of (θ, q) for the data and for the model. The model data are at level 19 (roughly 33 m), while the FIFE surface data are at 2 m. The numbers denote time in GMT where 12 denotes an average for the hour 1200–1300 GMT. Local solar noon is about 1820 GMT. We see that the FIFE data trace a path of almost constant q from the morning θ-minimum to the afternoon θ-maximum near 2100 GMT, when the surface starts cooling. The EC model data, however, move towards a warmer and drier diurnal cycle with time, and reach a maximum temperature later, near 2300 GMT. The isopleths of equivalent potential temperature, θ_E, show that the BL reaches an afternoon maximum in θ_E of 307 K in both model and data. We shall find contrasting results in some August averages (see Fig. 12, later).

Conditions are very dry in October: the surface LH flux is small, and BL mixing ratios are around 4 g kg^{-1}. In the next section we shall show some August comparisons when the observed evapotranspiration is large. This shows up other errors in the model, related to the evaporation and soil-moisture balance and to BL-top entrainment.

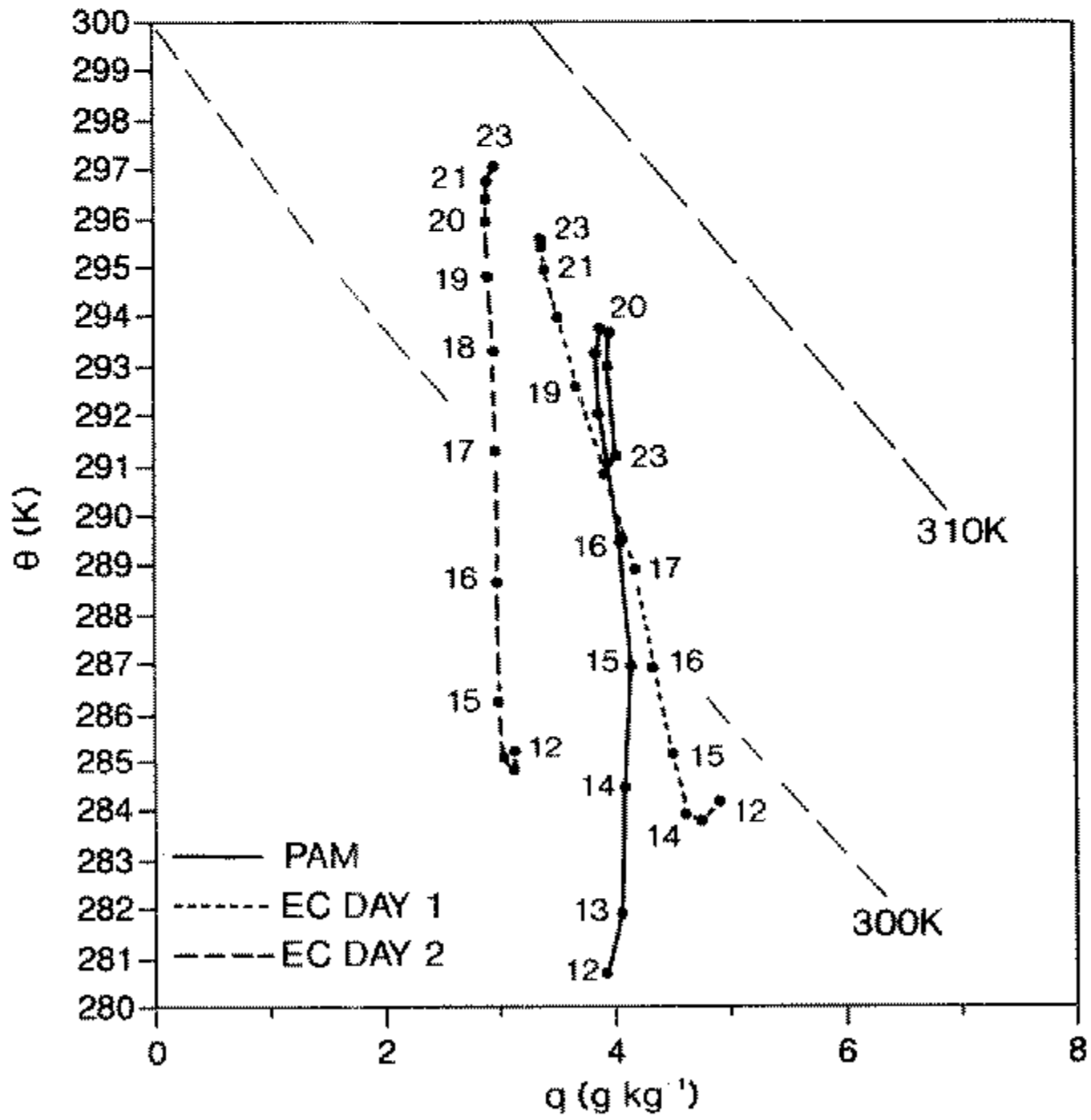

Figure 8. Day-time (θ–q) plots for data at 2 m and ECMWF model, level 19 (33 m), for 7-day October average. Isopleths of equivalent potential temperature are shown as long dashes. Numbers are hours in GMT; 12 denotes an average for the hour 1200–1300 GMT.

(*b*) *August comparison*

The second comparison covers the period from 6 to 21 August 1987. Two sets of model analyses were available: the operational analyses, as in October, and the exper-

imental analyses discussed in section 3. Although we looked at comparisons for individual time-periods we shall show a 9-day forecast composite from both analyses for a set of mostly sunny days with little rain. This selection was not as easy as in October, because of significant differences in cloud and rainfall between the observations and the forecasts from the two model analyses. There are 12 days in the data with little cloud and no significant day-time rainfall: August 6, 7, 9, 10, 11, 14, 15, 16, 17, 19, 20 and 21. August 8, 12, 13 and 18 were rainy days in the data and in both model forecasts. Of the 12 dry days in the data, three have significant rainfall in the forecasts from the experimental analyses (August 11, 14 and 19), leaving only 9 which are rain-free in these forecasts. However, it is clear that many of these had significantly more cloud in these model forecasts. Thus even the selection of these days suggested that the forecasts from the experimental analyses had two biases in August: more frequent day-time rain and cloud. Consequently we chose for our August composite the nine 24-hour time periods starting at 12 GMT for August 6–7, 9–10, 15–17 and 20–21. We used the same time periods for both sets of forecasts to facilitate comparison. However, there are significant differences between the different forecasts. For example, in the forecasts from the operational analyses, there is a little rain on the Day 1 forecasts for August 16 and 17, which are dry in the data and in the forecasts from the experimental analyses. These differences in rainfall in the model forecasts appear again to be related to the periods when the BL in the model is too moist (see later).

(i) *Composite August forecast from the operational analyses*. The comparison of the composite August forecast with the operational analyses, not surprisingly, confirms the model errors identified in section 4(a) for the October comparison of forecasts from the operational analyses. Many of the figures are omitted. The observed surface albedo is a little lower in August (when the vegetation is greener) by about 2%, and hence closer to the fixed 0.16 of the model. Figure 9 shows the net radiation comparison. The label OP39 denotes that these forecasts were made with cycle 39 of the EC model from the operational analyses. The higher curves are again the EC model, although the difference is not as large as in October because more cloud in the model compensates for the higher incoming solar flux. It is still true that on the rare day (such as August 9) when the model is cloud free, the incoming solar flux at noon is 10% higher than any of the FLUX observations in August, suggesting the same clear-sky bias as in October.

Figure 10 shows the SH and LH comparison. The model mean SH is too high, and LH flux is too low in comparison with the data. The phase-lag caused by the large morning ground heat flux (which peaks around 200 $W m^{-2}$) is again present (not shown). Figure 11 compares evaporative fraction (LH/(SH + LH)). The higher pair of model curves labelled EX39 (from the experimental analyses) will be discussed in the next section. The evaporative fraction in the forecasts from the operational analysis, labelled OP39, is too low; and it stays flat rather than rises in the afternoon. We shall see later (section 4(e)) that this is linked to the day-time fall in the model soil moisture. Superficially the surface flux comparison is certainly better than in October, when the model LH flux was zero. However, these averages give an incomplete picture. The spread of LH flux and evaporative fraction in the model is huge compared with the data. There are days (6 August) when there is almost no evaporation in the model ($<15 W m^{-2}$), and others after rain when the LH flux approaches 600 $W m^{-2}$. In the data, however, the range in August is much narrower (from about 250–420 $W m^{-2}$). This difference is related to the model soil-moisture fluctuations, and we shall discuss it in more detail in section 4(e).

The 2 m temperature comparison is similar to that in October, so we omit the figure. The model is generally warmer in the mean, and warms from Day 1 to Day 2 of the

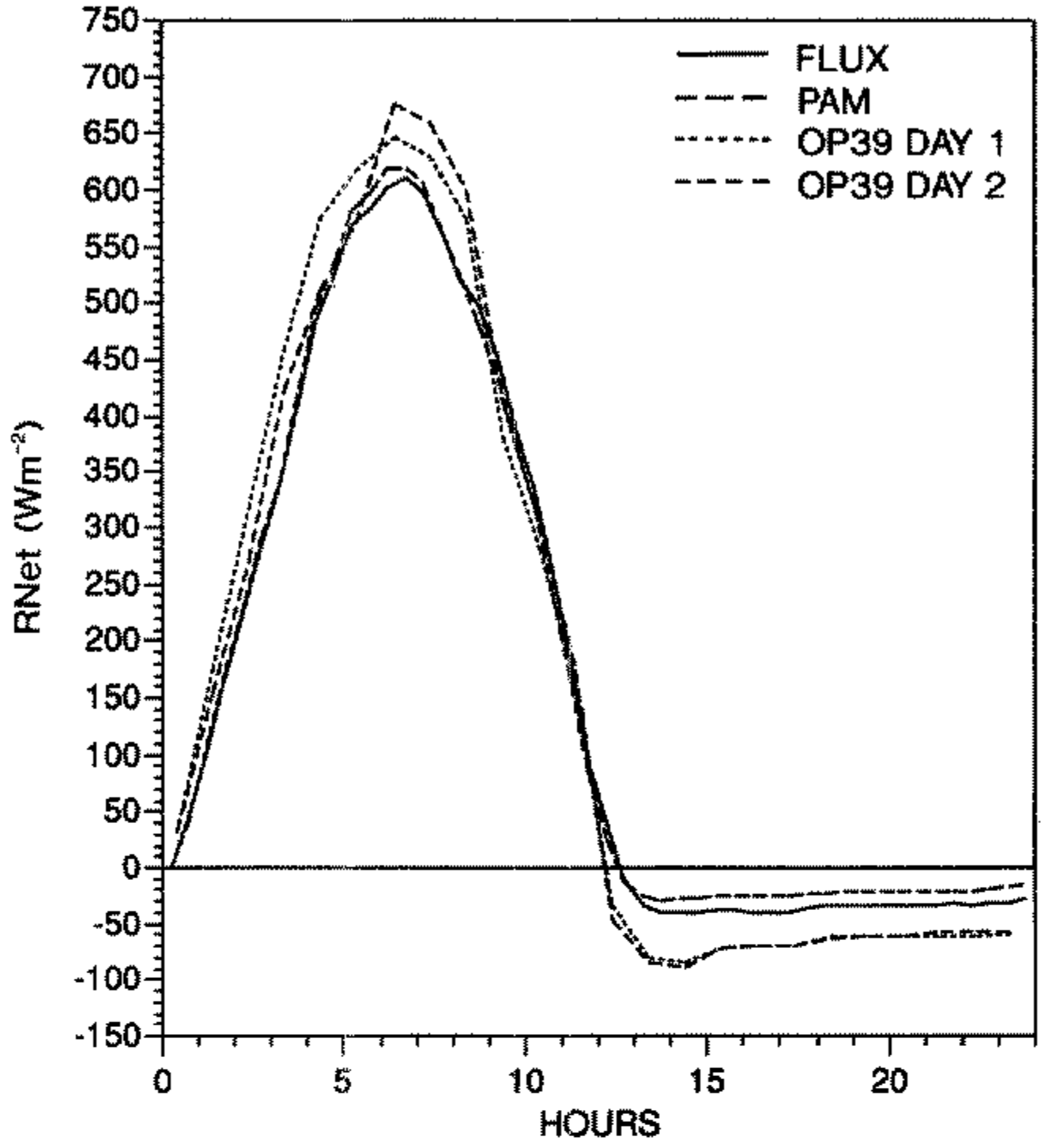

Figure 9. Net radiation (RNet) comparison for OP39 9-day August average with averages for the surface PAM stations and the FLUX average from the surface-flux stations.

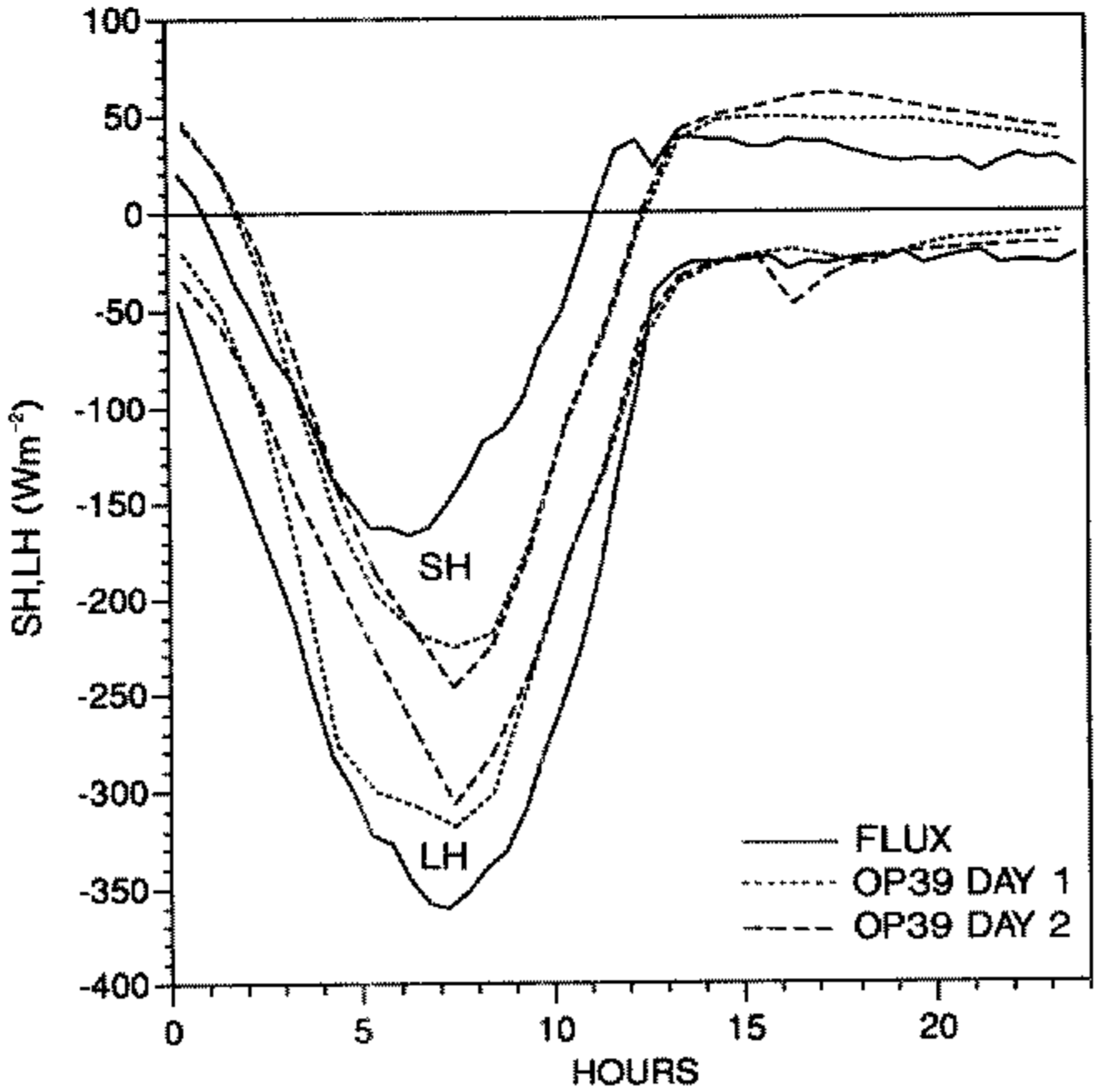

Figure 10. As Fig. 9 but for sensible- and latent-heat flux (SH and LH respectively).

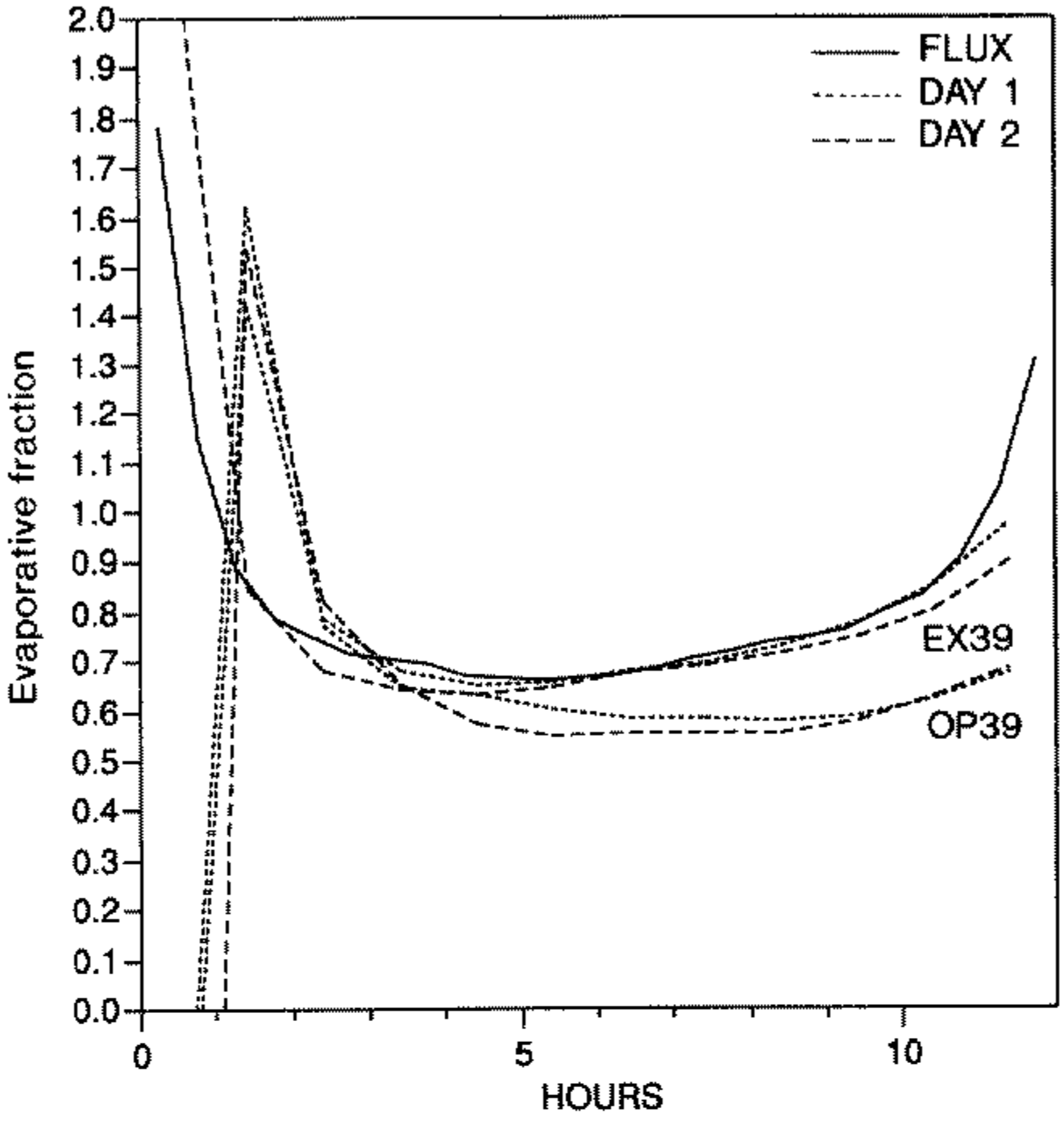

Figure 11. Day-time evaporative fraction for data, OP39 and EX39 averages.

forecast. As might be expected, on dry days with very little evaporation in the model, such as 6–7 August (not shown), the 2 m temperature reaches extreme values, over 40 °C, while the observed temperatures on those days reached a maximum of 33–34 °C. The difference between the observed surface (skin) and 2 m air temperature is again larger in the data than in the model, although the differences are smaller than in Fig. 6 because the surface SH fluxes are less.

Figure 12 summarizes the near-surface diurnal cycle on a (θ–q) plot: the observations are at 2 m, while the model values are at level 19 (near 33 m). The two curves labelled EX39 (from the experimental analyses) will be discussed in the next section. The composite forecast from the operational analyses, labelled OP39, shows some similarity with Fig. 8 for October. The operational analysis is too moist, and there is a sharp drying on Day 1. This continues on Day 2 of the forecast, giving a final state in the OP39 composite at sunset on Day 2, which is significantly warmer and drier than the observations, with little difference in θ_E. Note, however, that there is a morning maximum in θ_E on forecast Day 1, which is probably associated with the extra rain seen during these periods in the model.

(ii) *Composite August forecast from the experimental analyses*. The preceding section shows the comparison of a composite August forecast from the operational analyses. This drifts towards too warm and dry conditions near the surface. We shall see later that this is related to the dry specification of the 'climate layer' soil moisture in the operational analyses. This was made apparent to us because we also made forecasts from experimental analyses for August 1987, for which we use the label EX39 on the figures. As mentioned earlier (but unknown to us when we began this work), these analyses had by mistake values for the climate-layer soil moisture and temperature fixed at cool, moist June values. (These reanalyses also used cycle 39 of the EC model.) Although this climate temperature is too cold, the moist June soil climate is in fact closer to the observations than the dry August climate in the operational analyses. The difference between the

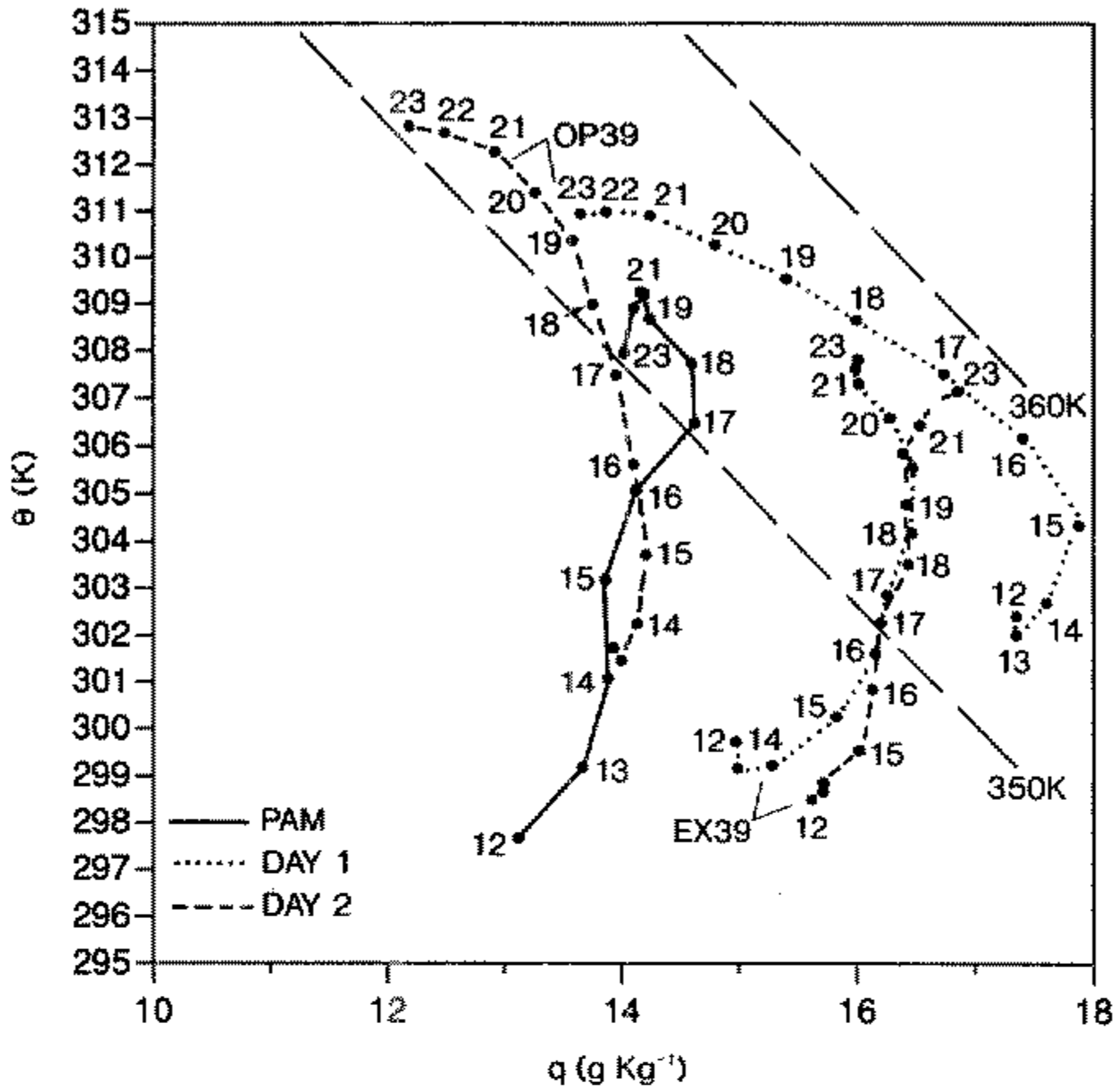

Figure 12. As Fig. 8 but for data, OP39, and EX39 August averages.

forecasts from these two analyses is instructive. It helped to identify clearly two new errors in the model, one associated with the lack of BL entrainment, and the other with weaknesses in the soil-moisture formulation.

We averaged the same nine August days from the EX39 forecasts as from the OP39 forecasts. Figure 13 shows the net radiation comparison between the data and the EX39 composite. In contrast to Fig. 9 (showing the data and the OP39 composite) the model now has less incoming net radiation than the data. This is due to an increase in cloudiness in the model, associated with a moister BL (see below). Figure 11, presented earlier, shows the day-time evaporative-fraction comparison between the flux data and both forecast composites. EX39 is much closer to the flux average (and so are the corresponding SH and LH fluxes (not shown)). The average does not show, however, that the range in the evaporation is also greatly reduced in the forecasts comprising EX39. The evaporative fraction near local noon on 6–7 August (Day 2) is now 0.42 for the EX39 forecasts whereas it was 0.03 for the OP39 forecasts. We shall return to this later (Fig. 19).

The diurnal cycle of near-surface temperature and mixing ratio is quite different for EX39 than for OP39. Figure 12 compares them on a (θ–q) plot. Whereas, in comparison with the data, OP39 moves towards a warmer, drier afternoon state, EX39 moves towards a cooler, moister state, with an afternoon maximum of θ_E that is 4–5 K higher than the data. Since the surface SH and LH fluxes for EX39 agree quite well, this suggests another error in the model. The surface fluxes increase θ_E in the BL. If the afternoon equilibrium has too high a θ_E, this means that the downward mixing of low θ_E air in the model must be too low. In fact the EC model has very little BL entrainment, and, as we shall see in the next section, the biases in θ_E and q in Fig. 12 are related to BL depth.

(c) *Boundary-layer profile and height comparison*

The August forecast averages from the two analyses differ significantly in BL structure and evolution. Near the surface (level 19 at 33 m), Fig. 12 shows that OP39

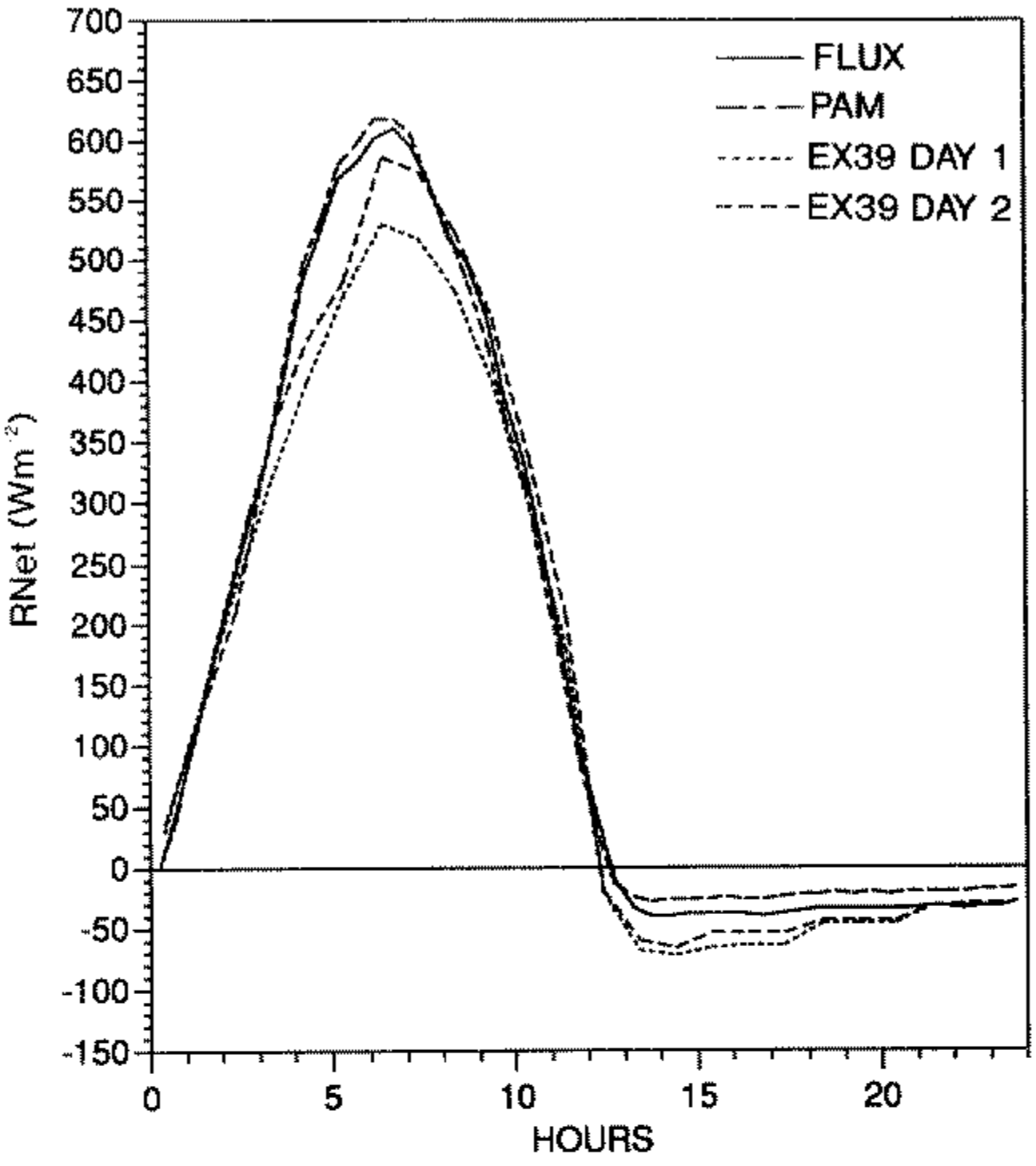

Figure 13. As Fig. 9 but for EX39 August average.

moves towards a warm and dry state (from a too moist initial condition), while EX39 moves towards a cooler, moister state than the data. The BL profiles reflect these drifts. Figures 14 and 15 show the moisture profiles for OP39 and EX39 compared with averaged sonde data. The corresponding θ profiles (not shown) show that the BL is too warm for the OP39 average and too cool for EX39, as expected from Fig. 12.

The model profiles are hourly averages, for the hour starting at the time shown. For the observations we used the radiosondes, which were launched at roughly 90-minute intervals on these nine days (the mean launch times are shown). The BL profiles (for both data and the model) were scaled in pressure using BL depth, and interpolated to scaled pressure levels before averaging, as discussed in section 2. This preserves the vertical structure within the BL in the composite (Betts 1976). For the model, which has a relatively coarse vertical resolution of order 60 mb, this definition of BL top is much less exact. We chose the middle of the first stable layer, found by lifting a buoyant parcel from the lowest model level, using a method proposed by Troen and Mahrt (1986). As a result of this coarse vertical resolution the model averages have much smoother profiles.

The BL depth is significantly different for the two averages. Figure 16 shows BL top, as a function of time, for the data and for the two EC averages, defined as the middle of the first stable layer. The forecasts from the operational analyses have a much higher BL top, close to that of the data, while in the forecasts from the experimental analyses the BL top grows at barely 60% of the rate observed. The model's surface latent-heat fluxes from both analyses are smaller than the data. The different behaviour of q with time in Figs. 14 and 15 is related to the difference in BL growth. Cycle 39 of the EC model has very little diffusion through stable layers, since diffusion coefficients are calculated using a local Richardson number closure (Louis 1979). Hence there is effectively no entrainment at the BL top. The BL does grow by encroachment as the

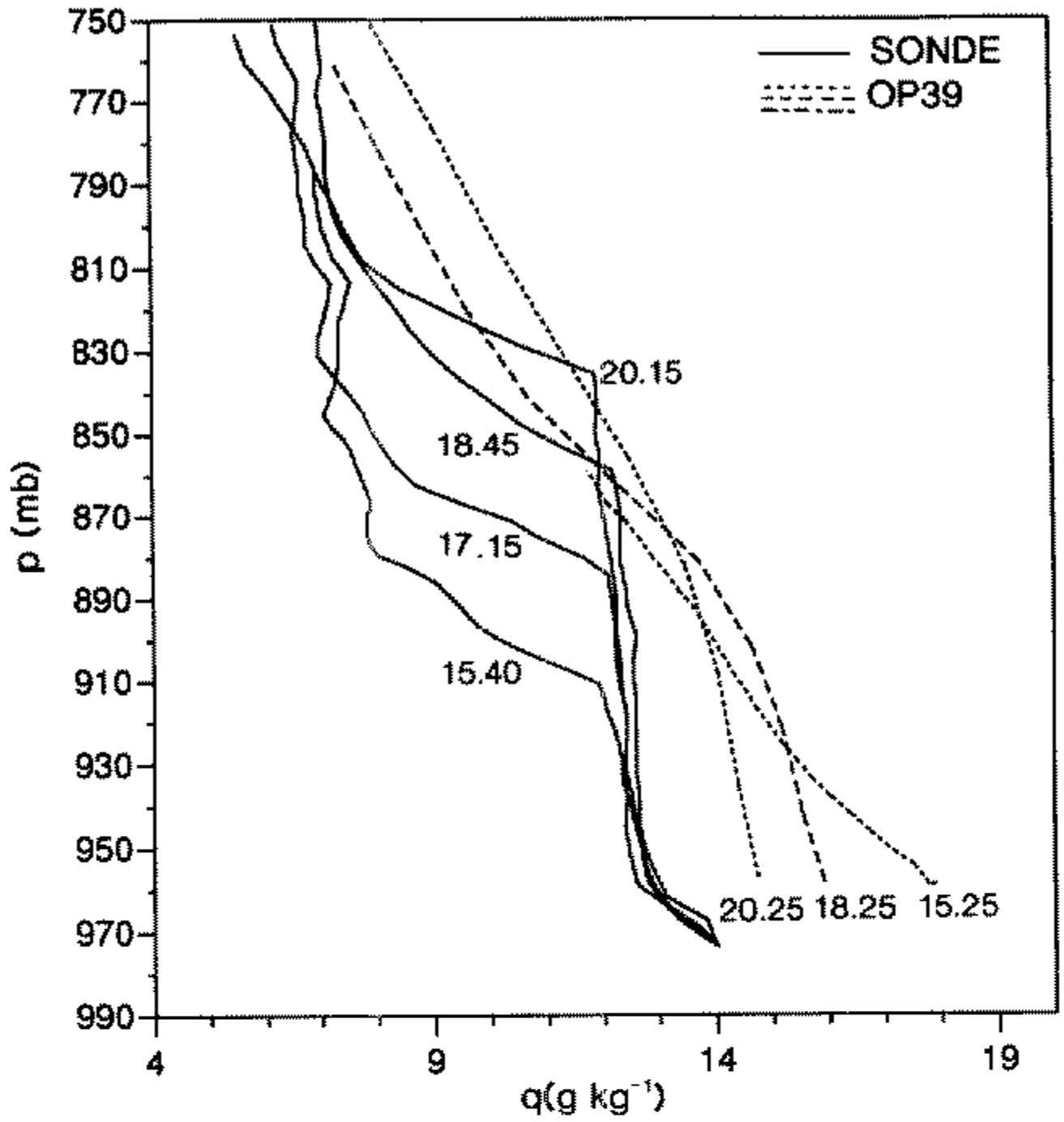

Figure 14. Comparison of boundary-layer profiles of mixing ratio, q, for 9-day August sonde averages for 1540, 1715, 1845, and 2015 GMT with average OP39 Day 1 profiles at 1525, 1825 and 2025 GMT.

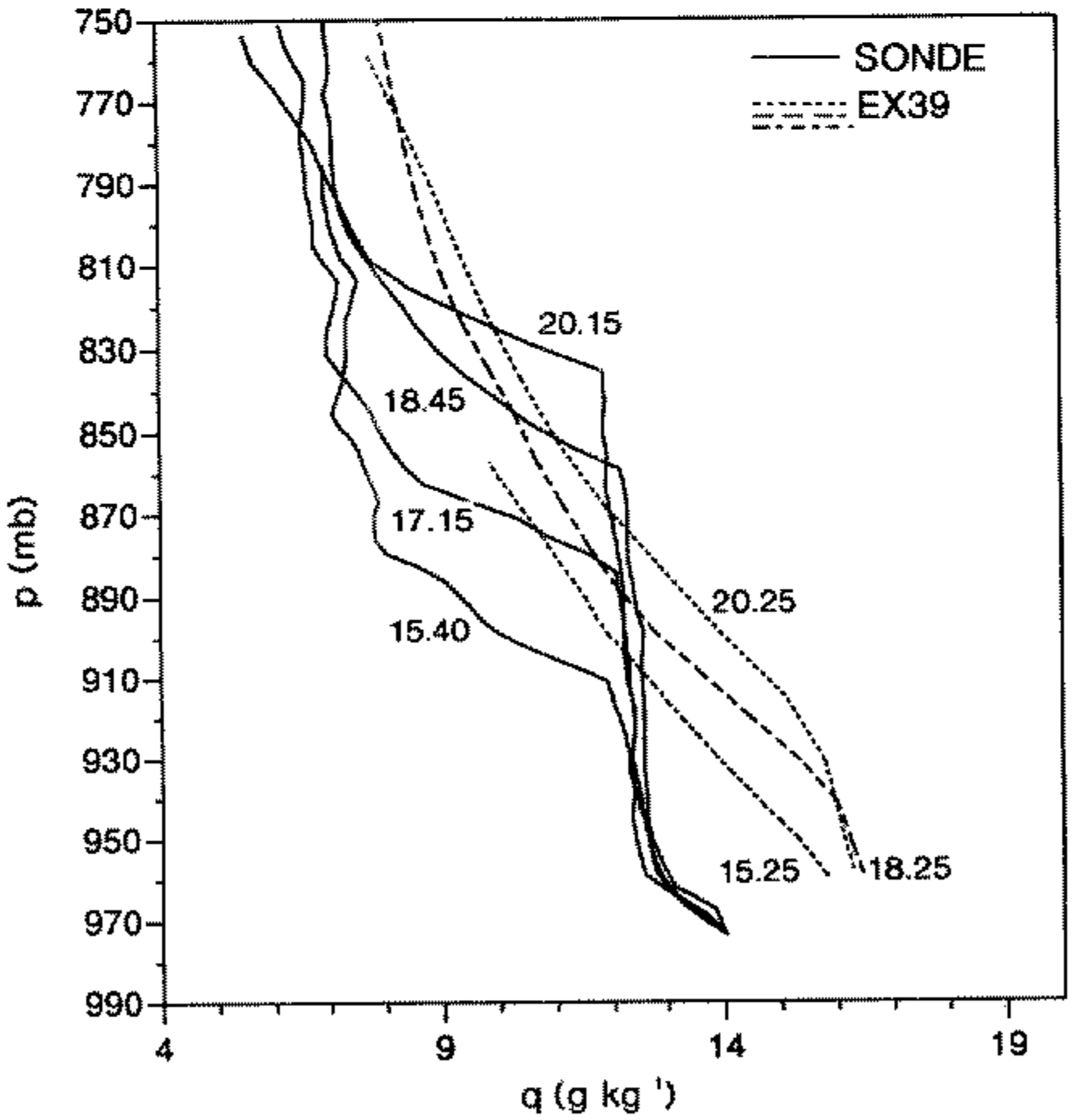

Figure 15. As Fig. 14 but for EX39 Day 1 averages.

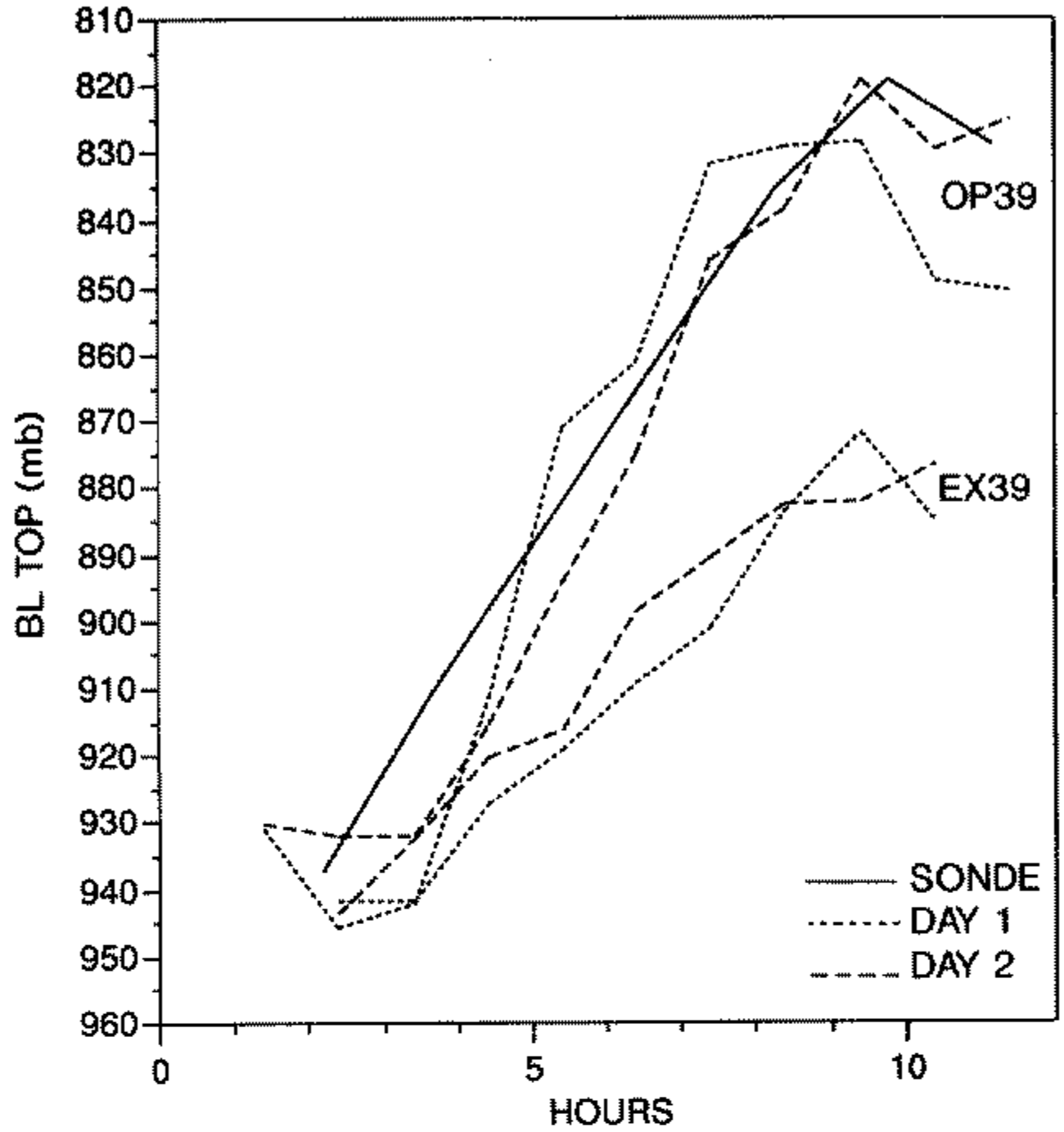

Figure 16. Comparison of boundary-layer (BL) top for 9-day August average; derived from sonde data and Day 1 and Day 2 of EX39 and OP39.

surface warms. For EX39 the surface temperatures are low because of the cold subsurface climate temperature, and the surface SH flux is close to that observed, but a little low. Without entrainment the model BL grows much too slowly, and the mixing ratio drifts to a moist state since less warm dry air is incorporated into the BL. For OP39 the surface heat flux is too high because the soil is drier; the surface temperature is also too high, and these compensate for the lack of entrainment, and push the BL top by encroachment to roughly the height observed by the afternoon. The BL dries out from an initially too-moist analysis towards the observed structure. Neither average gets the early morning BL growth right because of the lag of the SH flux caused by the ground storage error (although the limited model vertical resolution may also be a factor).

In the data, the BL mixing ratio is a very stable balance between surface evaporation and BL-top entrainment of dry air (Fig. 14). To get these right in the model is not easy; it requires an entrainment parametrization, and the right surface energy balance, which itself depends critically on the soil moisture. Nonetheless it is critical to the model forecast performance, because biases in the model q and θ_E produce biases in the diurnal cycle of cloud and rainfall.

(*d*) *Comparison of mid-day evaporative fraction*

Over the grassland hills of the FIFE site the surface evaporation is controlled largely by evapotranspiration, except immediately after rain when the surface is wet. On successive days without significant rainfall, soil moisture falls. Natural grassland appears to maintain a high level of evapotranspiration for long time-scales: of order 7–10 days or longer (see Kim and Verma (1990) for FIFE, and Gash *et al*. (1991) for fallow Sahelian savannah). It appears that the model parametrization of evaporation has a shorter time-scale of only a few days. This direct comparison is not easy to make, however, because

of differences in rainfall and cloudiness between model forecasts and the data. In this section we shall show some selected periods in July. These forecasts were from the experimental analyses for July. The fact that this used the June rather than the July deep-soil climate does not affect our conclusions significantly. The left-hand scale of Fig. 17 shows the evaporative fraction, defined as LH/(SH + LH), averaged for the period 1600–2000 GMT (centred near local solar noon: 1820 GMT) from the surface flux data and selected periods of the EC forecasts. 1–3, 9–11 and 14–16 July were days with little or no rain in FIFE. For 1–4 July the EC plots are for the first day of the forecasts for 1–3 July (it rained on 2 and 3 July in the model when these were the second forecast days) and for the second day forecast for 4 July. A significant decrease in evaporative fraction is seen over this 4-day dry period. In contrast, in the data for 1 and 2 July, the evaporative fraction is constant; it rises on 3 July because of cloud cover near local noon.

For the period 9–16 July we show the average evaporative fraction in the model for both forecasts for that date, and we draw attention to two periods. For 10–11 July the evaporative fraction fell more in the model than in the data (both periods were without rain in both model and data). It rained on 12 July in the model, and the evaporative fraction fell steadily from 12–16 July as shown. The data show a little rain on 12 and 13 July and then 14–16 July was dry also. IFC-2 of FIFE ended on 11 July, but a few flux stations collected data during this inter-phase period. The data from 12–20 July labelled 'UK' (see Stewart and Verma 1992) show that the noon evaporative fraction fell only slightly by 20 July. There is no significant rain in this period except for showers on 12–13 July and 17–18 July. It is clear from these three periods (and 5–7 August, not shown) that the evaporative fraction in the model falls more rapidly than the data on consecutive dry days.

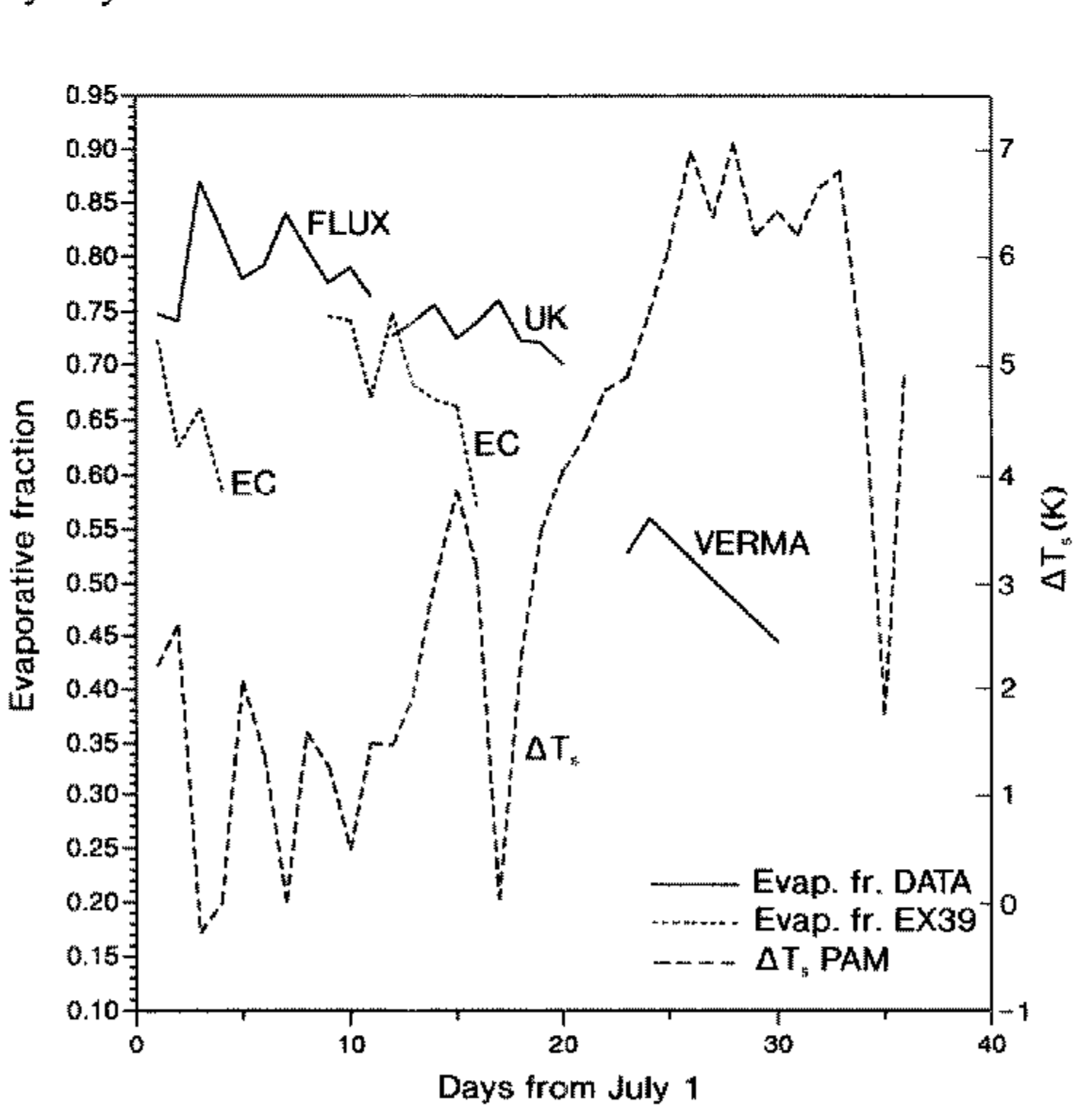

Figure 17. Comparison of mid-day evaporative fraction from observations and the ECMWF model (left scale). Observed difference, ΔT_s, between skin temperature and 2 m temperature for 1 July–5 August (right scale).

There was no rain in FIFE from 19 July–2 August 1987. Data from three days at one site are shown (Kim and Verma 1990). Unlike the period 12–20 July, by 23–30 July the evaporative fraction (at this different site) had fallen substantially as the soil dried. Figure 17 also shows (right-hand scale) the difference, ΔT_s, (for 1600–2000 GMT) between the radiometric surface temperature and the 2 m air temperature (averaged over the FIFE site from the PAM data). This qualitatively reflects the rise and fall of evaporative fraction with each rain episode. We can follow the rise of ΔT_s through the dry period, until the next rainfall on 3–4 August. After 20 July, ΔT_s continues to rise for a further six days, and then remains steady at about 7 K for about a week. During this period the wind speed fluctuated in the range 3–7 $m\,s^{-1}$. This is the time period when the Verma data show evaporative fraction ≈ 0.5.

Figure 17 (using data from Kim and Verma (1990) as well as Gash *et al.* (1991)) suggests that the response time before grassland vegetation becomes stressed, and evaporative fraction falls, is more than a week. The time constant for this process in the model is only a few days. The reason is the coupling between soil moisture and evaporation in the model. The unstressed canopy resistance to evaporation in this version of the EC model is only 25 $s\,m^{-1}$. The FIFE data (Kim and Verma 1990) gave larger values: 75 $s\,m^{-1}$ in the unstressed conditions on 11 July, rising to 300 $s\,m^{-1}$ in the dry, stressed conditions of late July. In the model the canopy resistance rises, and evaporation falls, as the mean soil moisture in the two subsurface layers (7 and 42 cm deep) falls below 60% of the field capacity. The 7 cm layer dries quickly, giving a short time constant for the fall of the evaporative fraction. Kim and Verma (1990) and Gash *et al.* (1991) show that the vegetation draws on a much deeper reservoir of soil moisture. In the model the reservoir of water in the 42 cm layer is controlled not by precipitation but largely by diffusion of moisture from the model's climate layer. This is explored more in the next section.

(*e*) *Soil moisture and evaporation in August*

Figure 18 shows how the different daily cycle of evaporation in the two sets of forecasts is controlled by the soil moisture and the different deep-climate values. The left-hand scale is fractional volumetric water content. The right-hand scale is that actually used in the EC model for soil moisture: cm of water per 7 cm soil layer. The arrows at 1.2 and 0.6 (0.171 and 0.086 as a volumetric fraction) are the two critical limits in the model at 60% and 30% of the soil field capacity, corresponding to unstressed evapotranspiration and the wilting point of the vegetation, where evapotranspiration ceases (Blondin 1991).

The broken lines at 0.09 and 0.253 (volumetric fraction) are the very different *specified* climate soil moistures for the OP39 forecasts with an August climatology from Mintz and Serafini (1989), and EX39 which retained the moist June climatology. The solid lines are the deep-soil moisture. For OP39 the value is close to the climate value, and the evapotranspiration cut-off at 0.086. For EX39 diffusion from the very moist climate layer keeps the deep-soil moisture near 0.14. This diffusion of water from the climate layer is a major contribution to the soil-moisture budget. Driven by the 0.11 difference in soil moisture between the climate layer and deep-soil layer (and the model hydraulic diffusitivity of $10^{-7}\,m^2\,s^{-1}$), it contributes to an evaporation of 2.7 mm day^{-1}, or a diurnally averaged latent-heat flux of 80 $W\,m^{-2}$. Thus the model's soil-water budget is not closed.

The curves, which show a day-time drop of soil moisture, are for the shallow 7 cm soil layer. EX39 is higher on Day 2 than Day 1, and the reverse for OP39 because of the different diffusion from the deep layer. The day-time fall of soil moisture for EX39 is reduced for the same reason. The stomatal resistance (and hence evapotranspiration) is

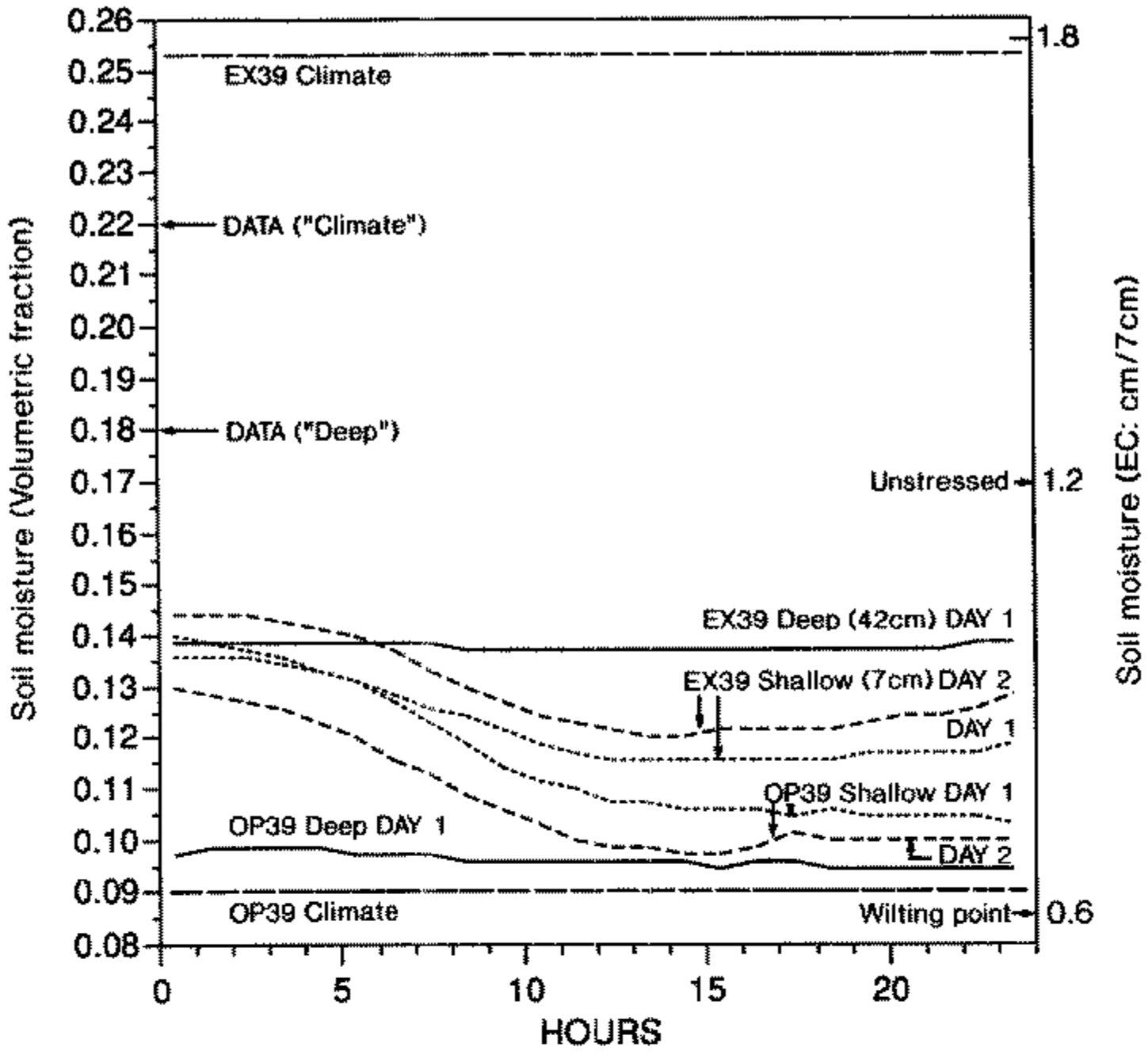

Figure 18. Comparison of climate values and diurnal cycle of deep-soil and shallow-soil moisture for 7-day August averages: EX39 and OP39.

determined in the model by the simple average of the soil moisture in the deep and shallow layers, and their relation to the unstressed and wilting-point thresholds shown. Thus it is clear from Fig. 18 why OP39 has both a smaller evaporative fraction, and a larger fall of evaporative fraction, during the day.

The soil and evaporation model has several underlying problems. The shallow 7 cm layer has a large day-time moisture fall. On successive days without rain it dries out quickly. The deeper 42 cm layer has a larger capacity, but it is not replenished directly by rainfall, only by hydraulic diffusion from above and below. This has a 10-day time-scale. (The hydraulic diffusivity in the operational model is fixed.) Since the shallow layer dries out in a few days after rainfall, the soil moisture in the deeper layer changes little, and its mean is controlled primarily by diffusion from the prescribed value in the climate layer. This value was taken from Mintz and Serafini (1989), where it was calculated as a mean for the root-zone soil moisture, rather than a value below 49 cm as used in the EC model. Since the 42 cm layer is never replenished significantly by rainfall, the model cannot maintain high evaporation for more than a few days without rain, unlike natural grassland. Furthermore, the prescribed deep climate has a major control on the model's diurnal cycle through its control on the deep 42 cm layer moisture. A predicted climate layer is needed, and a faster mechanism for getting rain into the deeper layers (where it can be stored), such as a hydraulic diffusivity which depends on soil moisture.

Soil-moisture comparisons with the data are less straightforward. Soil moisture was measured by a gravimetric method at roughly 100 locations almost daily during the IFC for two depths, 0–5 cm and 5–10 cm. For a few dates a deep-soil-moisture profile is available at a site. Figure 18 shows measured soil moisture (from the 31 July profile in Kim and Verma (1990)) at two depths, corresponding to the EC model's 42 cm deep layer, and the climate layer below. This observed 'climate' value at the beginning of

August is much closer to that assumed in EX39 than OP39, and the observed 'deep' value (towards the end of the late July dry spell, but before any of the August rain) is above the EX39 August average.

The soil moisture in the FIFE data for the first 10 cm varies considerably in August, between 0.16 and 0.29, with rainfall events. The mean value is 0.223 for the nine August days in our composite, much higher than the EC model value. The maximum mean volumetric soil moisture in FIFE is, however, about 0.335 for the first 5 cm; about 17% above the value of 0.286 above which the EC model removes soil water by runoff.

Figure 19 shows a scatterplot of the relationship between mean soil moisture and average evaporative fraction near local noon (1600–2000 GMT) for the FLUX data and the two sets of model forecasts. The mean soil moisture is the average of the 7 and 42 cm layers for the EC model (since this determines stomatal resistance). For the FIFE data we have no detailed time series below 10 cm, so we averaged the daily-varying 0–10 cm mean and a fixed value of 0.18, corresponding to the 31 July deep profile in Kim and Verma (1990), to give a mean soil moisture roughly comparable with the EC average. The OP39 forecasts show the wide range of evaporative fraction, and the tail towards zero evaporation as the 7 cm shallow-layer moisture dries towards the wilting-point threshold. The EX39 forecasts have a higher evaporative fraction because both the deep-soil and shallow-soil moistures are higher. The FLUX data are for 6–21 August and the 23 and 30 July measurements are from Kim and Verma (1990). (July 30 is the driest soil-moisture point.) The data indicate a weak fall of evaporative fraction with soil moisture. As mentioned earlier, the FIFE soils have a 17% larger maximum soil wetness (at saturation) than the value used in the EC model; this may partially account for the displacement of the data towards larger values of soil moisture. The three consecutive days, 9, 10, and 11 August, are marked for the observations and Day 2 of the two sets of forecasts. For OP39 the dramatic fall of evaporative fraction on consecutive dry days

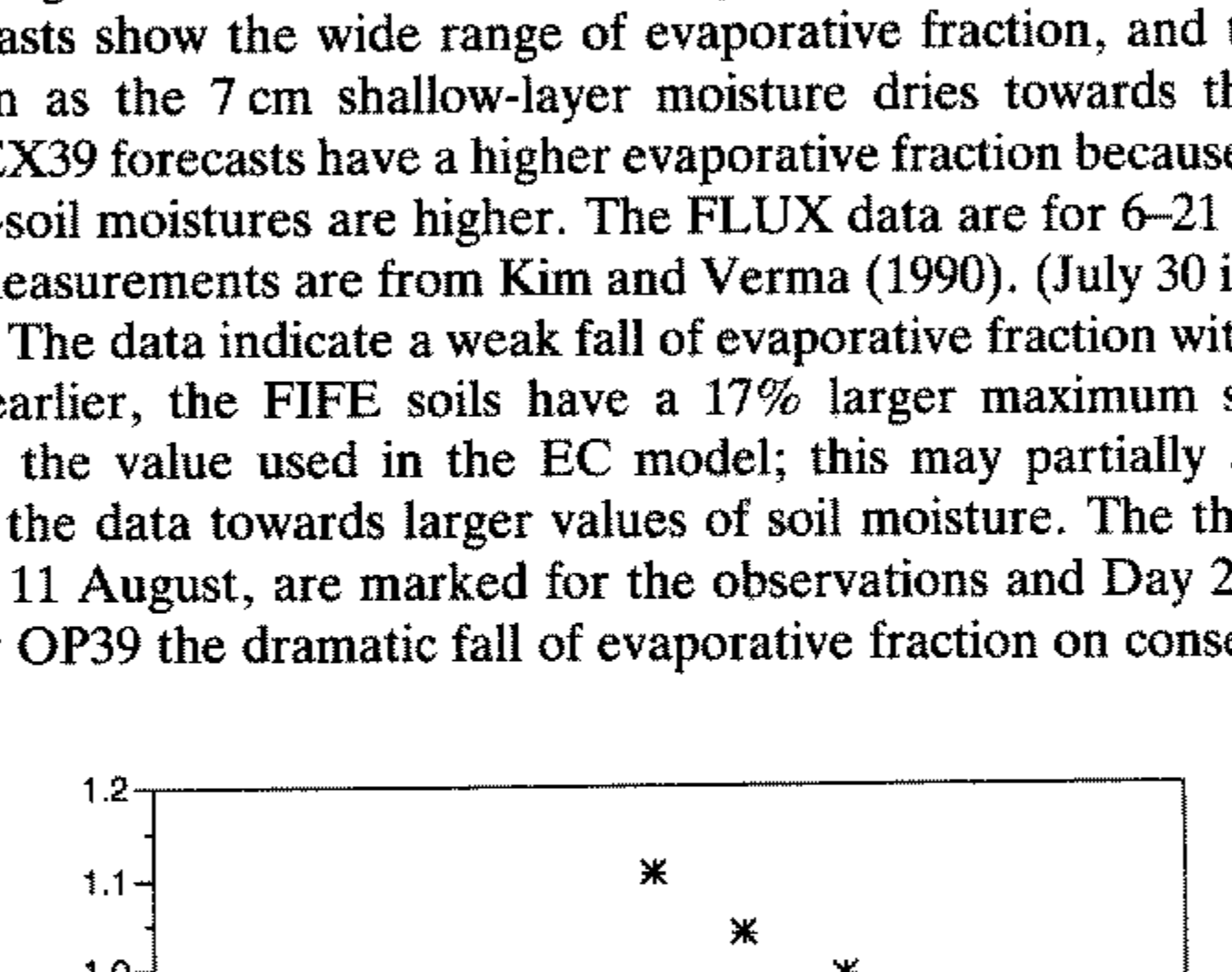

Figure 19. Scatterplot of evaporative fraction for August forecasts (EX39 and OP39) and data against mean volumetric soil moisture. (See text for explanation of numbers.)

is apparent, since the soil moisture is close to the wilting point. EX39 shows a much smaller change (it rained in this 11 August forecast), and in the data no drop of evaporative fraction is visible. The very different distribution of points between the OP39 and EX39 forecasts makes it clear that evaporation in the EC model is controlled too much by the specified climate soil moisture (which had the low value of 0.09 in the OP39 forecasts). Improvements in this soil-moisture model are under development.

5. Discussion and conclusions

We have intercompared the observed diurnal cycle over the 15 × 15 km FIFE area in Kansas, using data from the summer and fall of 1987, with the simulated diurnal cycle in the ECMWF model at the closest model grid point. Several systematic model errors have been identified from this comparison.

The incoming solar radiation at the surface under clear skies in the model appears high, perhaps by as much as 10%. This difference is much too large to be explained in terms of the water-vapour differences between model and data. So far three possible small biases in the model have been identified; they are each of order 1–2% and they are all additive. The parametrized version of the short-wave radiative code has an incoming flux 1–2% higher than a more exact narrow-band model (Morcrette, personal communication). In addition the code does not at present include absorption in the short wave by either the water-vapour continuum or aerosols; each of which might account for another 1–2% reduction in the incoming clear-sky short wave at the surface. On some days the aerosol absorption may be larger. This model clear-sky bias in the short wave is, however, partially offset by higher day-time cloudiness in the EC model, especially during the summer forecasts from experimental analyses.

The ground heat flux in the model is much too high during the day-time heating cycle, reaching values in the morning of over 200 $W m^{-2}$ under clear skies. The chief reason for this is the large thermal capacity of the 7 cm thick top ground layer. This must be heated before surface instability can transfer sensible heat to the atmosphere. This ground heat-flux error is amplified by a time-truncation problem in the model. One consequence is that the model's sensible- and latent-heat fluxes lag by about 2 hours because of the slow thermal response of this 7 cm soil layer. In addition, the range between surface maximum and minimum temperatures is reduced. The diurnally averaged heat flux into the ground is also generally too high. There is, therefore, a tendency under clear skies for the ground to heat up on consecutive days, and for this to bias the surface 2 m temperature. The difference between surface temperature and air temperature is too small in the model. This is in part associated with having the same roughness lengths for heat and momentum in the model, while the data suggest that the roughness length for heat is at least an order of magnitude less than that for momentum (Betts and Beljaars, personal communication).

The surface evaporation formulation has some apparent deficiencies. In October 1987 (using the operational analyses) the model has no evaporation, since the mean soil moisture is below the model wilting point, whereas the observations show low, but significant, continued evaporation. The low value of the specified soil moisture in the climate layer is the primary cause. In the summer season the observed canopy resistance to evaporation in unstressed conditions is greater than the value specified in the model. For this period two analyses were available in the summer, which in August have very different specified climate soil moistures. As a result we were able to explore explicitly the control of the soil model on evaporation. Several underlying problems were apparent. The shallow 7 cm soil layer has a large day-time moisture fall. On successive days without

rain it dries out quickly. In the model it takes only a few days (after rain) for the evaporative fraction to fall from ≈0.75 to 0.55, whereas the time-scale for this transition for the grassland ecosystem of FIFE is longer, perhaps 7–10 days. Natural vegetation appears to be able to draw on deeper resources of soil moisture (Kim and Verma 1990; Gash *et al.* 1991), and thereby to continue high evapotranspiration for longer before reaching a stressed condition. The model has of course only a simple representation of this process. It calculates the canopy stomatal resistance from the average soil moisture in a 'root zone' in two ground layers (7 and 42 cm thick) where moisture storage is predicted. There is diffusion of moisture from the 'climate layer' beneath. The specified climate soil moisture greatly affects the equilibrium of the 42 cm layer, and hence the evapotranspiration. It is clear that a predicted climate-soil layer is essential to improve the model. The observed soil moisture in FIFE at the depths of the EC climate layer was much moister at the end of July (even after two weeks of no rain) than the EC August climate, taken from Mintz and Serafini (1989); their analysis was intended to give mean moisture for the whole root zone, not at the EC-model climate-layer depth. The EC model has also no mechanism for quickly replenishing its 42 cm deep-soil layer during rainfall. The fixed hydraulic diffusion coefficient sets the diffusion time-scale into the deep layer at about ten days. Since the 7 cm layer dries out much faster than this, the larger storage capacity of the 42 cm layer is never fully replenished, even after heavy rainfall. As a result the longer time periods of 7–10 days of sustained unstressed evapotranspiration without rain, that are observed in FIFE and other grasslands, are not possible in the model. The deep-layer equilibrium is controlled instead mostly by diffusion from the climate layer. For the EX39 forecasts from the experimental analysis, with a moist climate-soil layer, the climate-soil layer supplied 2.7 mm day^{-1} of water, equivalent to a diurnally averaged evaporation of 80 W m^{-2}.

In the forcasts from the experimental analyses (EX39) the surface fluxes were much closer to those observed than in the forecasts from the operational analyses (OP93). Yet the boundary-layer mixing ratio in these forecasts is biased high in August by about 2 g kg^{-1}. This is not due to excessive surface evaporation, but to a deficiency in the downward entrainment of dry air from above the boundary layer. Typically the model's BL in these forecasts reaches only 60% of the depth of the observed BL over the FIFE site during the day. Diagnostic studies of the FIFE data showed that BL-top entrainment was much higher than that predicted by many entrainment models (Betts 1992; Betts *et al.* 1990, 1992). Culf (1992) found similar high entrainment rates for BL growth over the West African Sahel, as did Dubosclard (1979), using data over France. In contrast, the BL in this version of the ECMWF operational model has effectively no entrainment: the BL grows primarily by encroachment. In EX39 the cool surface temperature (influenced by the cooler soil temperature in the climate layer and the greater cloudiness) reduces the encroachment. This lack of downward mixing of dry air from above the BL led to a significant moist bias in the BL mixing ratio in these forecasts. In turn this moist bias is probably related to the positive bias in both day-time cloudiness, and the frequency of precipitation shown in August EX39 forecasts. In contrast, in the OP39 forecasts from the operational analyses (with a dry climate-soil layer), the BL dries rapidly from an initial state that is too moist. This is because the surface LH flux is too low, and the high surface SH flux and high surface temperature deepen the BL simply by encroachment.

An experimental surface model is under development to correct many of these biases. A skin temperature and a different time-differencing scheme have been introduced to remove the large bias in the ground heat flux and surface temperature, and their consequences (Beljaars and Betts 1992). Different roughness lengths for heat and momentum have been added, based on Betts and Beljaars (personal communication).

The unstressed canopy resistance to evaporation has been increased to agree more closely with data. In addition a BL model with explicit BL-top entrainment is being tested to give a more realistic growth of the day-time BL in the model, and to reduce the biases in BL moisture. These model experiments will be discussed in a later paper. Improvements to the soil model are also under development.

Our main conclusion from this study is that relatively simple comparisons of the diurnal cycle over land with a high-quality data set can give much insight into the systematic errors of a global model, and suggest a strategy for model development.

ACKNOWLEDGEMENTS

A. K. Betts was supported by the National Aeronautics and Space Administration–Goddard Space Flight Center (NASA–GSFC) under Contract NAS5-20134 (Task 47), and the National Science Foundation under Grant ATM90-01960. This work was partly completed during visits supported by the ECMWF.

APPENDIX—*Data processing*

The raw data files are available at the NASA–GSFC as part of the FIFE Information System (FIS). Some of these data (for example the PAM data) are also available on CD-ROM. We shall discuss each data set in turn.

(*a*) *Surface PAM stations*

The surface PAM stations were PAM-II stations supplied by the National Center for Atmospheric Research (NCAR), with pressure (P_s), temperature (T) and wet-bulb (T_w) temperature sensors mounted at 2 m and an anemometer at 5.4 m, as well as ground temperature sensors at 10 cm (Tsoil1) and 50 cm (Tsoil2) below the surface.

Each station measured surface skin temperature (TSfc) with a downward looking radiometer, net radiation (RNet) with a net radiometer, and reflected solar radiation (SolRef), and recorded rain rate and accumulation from a tipping-bucket raingauge. A subset of stations (two before 10 August 1987 and then four) measured incoming solar radiation (SolDn), and long-wave radiation (LWDN) (two before October 1987 and then four). The archive data use the NCAR calibrations of the instruments.

Data filters. A set of filters was applied to reject bad data points and identify lines of bad data (such as produced by electrical noise). These are shown in Table A1.

TABLE A1. DATA FILTERS

Variable*	Date		
	26 May–24 June	25 June–21 Aug.	22 Aug–16 Oct.
SolDn ($W m^{-2}$)	−5 to 1200	−5 to 1200	−5 to 1200
SolRef ($W m^{-2}$)	−5 to 250	−5 to 250	−5 to 250
RNet ($W m^{-2}$)	−98 to 1000	−98 to 1000	−98 to 800
TSfc (°C)	0 to 55	10 to 55	−10 to 35
TSoil1 (°C)	9 to 30	18 to 32	9 to 30
TSoil2 (°C)	11 to 30	18 to 30	11 to 30

* For explanation see text.

T and T_w were filtered to eliminate any data where T was less than T_w. The data were scanned for low values of surface pressure.

For both the radiation and thermodynamic data, further data editing was done by scanning the data and nulling-out obvious bad data manually. Some bad values will, however, have slipped through.

The mixing ratio (q) was calculated from T_w and P_s as follows:

$$Q_w = 622/[0.1631 \times P_s \times \exp\{-17.67 \times T_w/(T_w + 243.5)\} - 1]$$

$$q = Q_w - (1006/2501) \times (T - T_w)$$

where Q_w is the saturation mixing ratio at T_w.

Data averaging. All the station data that passed this editing were averaged for each date and time to give a site average, a standard deviation, and a count of stations in the average. The centre of the FIFE area is close to 39.05°N, 96.53°W. This compacted data set is available from the authors on diskette (Betts and Ball 1992).

(*b*) *Flux-station data*

The flux-station data came from a variety of instruments and investigators (for details, see FIS archives). The data set is still not in the final form, so we selected 13 stations with good time series of data to generate averages for three variables SH, LH, and RNet. A final average product based on a more objective selection of valid surface flux data using model studies is being produced by FIS and P. Sellers (personal communication). The 13 stations used for our average were five eddy-correlation stations with old (new) site numbers

16(4439), 22(4609), 26(8739), 28(6943), 30(4268),

and eight Bowen-ratio stations with site numbers

2(1916), 8(3129), 10(3414), 12(2915), 14(2516), 18(4439), 24(6912), 40(1246).

For the ground heat flux and other radiation variables we averaged all good data.

Data filters. The following range filters were used for the FLUX data. Only data within these ranges were accepted. The sign convention on LH, SH, and Grnd is negative for fluxes away from the surface. All fluxes are in $W\,m^{-2}$.

LH	−500 to 100 (latent-heat flux)
SH	−500 to 200 (sensible-heat flux)
Grnd	−300 to 150 (ground heat flux)
LWUP	100 to 600 (long wave up)
LWDN	100 to 600 (long wave down)
TSfcK	0 to 500 K.

RNet, SolDn and SolRef used the same data filters as shown in Table A1 for the PAM data.

Further data editing was done by scanning the data and nulling out obvious bad data manually. The remaining data for each date–time interval was then averaged to give a site average, a standard deviation, and a count of stations in the average: for SH, LH and RNet only data from the 13 stations listed above were used.

(*c*) *Consistency of the radiation data*

Averages of the archived radiation data for both the 'PAM' and 'FLUX' stations are shown. The net radiation averages agree closely during the day-time (to $< 15\,W\,m^{-2}$), although at night the FLUX measurements systematically show a slightly larger net outgoing radiation (by 10–20 $W\,m^{-2}$). The day-time solar averages also have systematic

biases: the FLUX average has a lower incoming solar radiation (by 3–6%), and a higher albedo (by 3%). The outgoing long-wave radiation measurements, corresponding to the radiometric surface temperature, agree to $<10\,W\,m^{-2}$; while the incoming long-wave radiation from the PAM average is systematically higher than the FLUX average at solar noon by about $20\,W\,m^{-2}$. Since all four radiation components are measured separately, we can sum these to give an $RNet_{calc}$, and compare this with the measured RNet as a consistency check.

The FLUX radiation averages, which have lower incoming solar radiation and a higher albedo, are internally much more self consistent: that is $RNet_{calc}$ agrees with RNet to $<20\,W\,m^{-2}$. For the PAM averages ($RNet_{calc}$ – RNet) reaches $110\,W\,m^{-2}$ at solar noon in August because of the larger contributions from SolDn and LWDN, and the smaller albedo. Although this comparison is compromised by the fact that not all radiation components were measured at all sites, the internal self-consistency (and agreement with both measurements of RNet) gives us more confidence in the FLUX radiation data.

(*d*) *Supporting surface data*

Other supporting data were used. A time series of digitized cloud camera data (photos every 40 min) gave high cloud cover and total cloud cover. A site-average soil-moisture time series was produced from the roughly 100 gravimetric samples taken for two subsurface layers (0–5 and 5–10 cm), sometimes daily, sometimes less frequently. These were converted from percentage of water by dry weight of soil to a volumetric fraction of water, using a mean bulk wet-soil density of 1.1.

(*e*) *Sonde data*

The sonde data are from radiosondes measuring temperature, wet-bulb temperature and pressure which were tracked by theodelite (see Sugita and Brutsaert 1990). The launch site was at 39°03′51″N, 96°32′30″W. The data are available from FIS as raw data, roughly every few mb, and interpolated to 5 mb standard levels. Whenever possible, sondes were tracked visually to 3000–4000 m. For this paper the raw data were scaled by BL depth, and then interpolated and averaged as discussed in the text.

References

Beljaars, A. C. M. 1991 'Numerical schemes for parameterizations'. *Numerical methods in atmospheric models, Vol. II*. Pp. 1–42 in ECMWF seminar proceedings, Sept. 1991

Beljaars, A. C. M. and Betts, A. K. 1992 'Validation of the boundary layer representation in the ECMWF model'. *Validation of models over Europe*. ECMWF seminar proceedings, Sept. 1992

Betts, A. K. 1976 Modelling subcloud layer structure and interaction with a shallow cumulus layer *J. Atmos. Sci.*, **33,** 2363–2382

1992 Budget analyses of the FIFE atmospheric boundary layer. *J. Geophys. Res. (Atmos)*, **97,** 18523–18532

Betts, A. K. and Ball, J. H. 1992 'FIFE-1987 mean surface data time series'. Available on diskette from author (Atmospheric Research, Pittsford, VT 05763)

Betts, A. K., Desjardins, R. L., MacPherson, J. I. and Kelly, R. D. 1990 Boundary-layer heat and moisture budgets from FIFE. *Boundary-Layer Meteorol.*, **50,** 109–137

Betts, A. K., Desjardins, R. L. and MacPherson, J. I. 1992 Budget analysis of the boundary layer grid flights during FIFE-1987. *J. Geophys. Res. (Atmos)*, **97,** 18533–18546

Blondin, C. 1991 Parameterization of land-surface processes in numerical weather prediction. Pp. 31–54 in *Land surface evaporation, measurement and parameterization*. Ed. T. J. Schmugge and J. C. André. Springer-Verlag

Culf, A. D. 1992 An application of simple models to Sahelian convective boundary-layer growth. *Boundary-Layer Meteorol.* **58,** 1–18

Dubosclard, G. 1979 A comparison between observed and predicted values for the entrainment coefficient in the planetary boundary layer. *Boundary-Layer Meteorol.*, **18,** 473–483

ECMWF 1988 'Parameterization of fluxes over land surfaces'. Workshop Proceedings, ECMWF, Reading, England (Available from ECMWF, Shinfield Park, Reading RG2 9AX, UK)

Garratt, J. R. 1978 Transfer characteristics for a heterogeneous surface of large aerodynamic roughness. *Q. J. R. Meteorol. Soc.*, **104,** 491–502

Garratt, J. R. and Hicks, B. B. 1973 Momentum, heat and water vapour transfer to and from natural and artificial surfaces. *Q. J. R. Meteorol. Soc.*, **99,** 680–687

Gash, J. H. C., Wallace, J. S., Lloyd, C. R., Dolman, A. J., Sivakumar, M. V. K. and Renard, C. 1991 Measurements of evaporation from fallow Sahelian savannah at the start of the dry season. *Q. J. R. Meteorol. Soc.*, **117,** 749–760

Geleyn, J. F. 1988 Interpretation of wind temperature and humidity values from model levels to the height of measurements. *Tellus*, **40A,** 347–351

Kim, J. and Verma, S. B. 1990 Components of surface energy balance in a temperate grassland ecosystem. *Boundary-Layer Meteorol.*, **51,** 401–417

Louis, J. F. 1979 A parametric model of vertical eddy fluxes in the atmosphere. *Boundary-Layer Meteorol.*, **17,** 187–202

Louis, J. F., Tiedtke, M. and Gelyn, J. F. 1982 'A short history of the operational PBL-parameterization at ECMWF'. Pp. 59–79 in Workshop on boundary layer parameterization. ECMWF, Nov. 1981. (Available from ECMWF, Shinfield Park, Reading RG2 9AX, UK)

Mahfouf, J. F. 1991 Analysis of soil moisture from near-surface parameters: A feasibility study. *J. Appl. Meteorol.*, **30,** 1534–1547

Mintz, Y. and Serafini, Y. V. 1989 Global monthly climatology of soil moisture and water balance. UNESCO studies and reports in hydrology

Sellers, P., Mintz, Y., Sud, Y. C. and Dalcher, A. 1986 A simple biosphere model (SiB) for use within general circulation models. *J. Atmos. Sci.*, **43,** 505–531

Sellers, P. J., Hall, F. G., Strebel, D. E. and Murphy, F. F. 1988 The First ISLSCP Field Experiment (FIFE). *Bull. Am. Meteorol. Soc.*, **69,** 22–27

Simmons, A. J. and Strüfing, R. 1981 'An energy and angular-momentum conserving scheme, hybrid coordinates and medium-range weather prediction'. ECMWF Tech. Rep. No. 28. (Available from ECMWF, Shinfield Park, Reading RG2 9AX, UK)

Stewart, J. B. and Verma, S. B. 1992 Comparison of surface fluxes and conductances at two contrasting sites within FIFE area. *J. Geophys. Res.* (*Atmos*), **97,** 18623–18628

Sugita, M. and Brutsaert, W. 1990 Wind velocity measurements in the neutral boundary layer above hilly prairie. *J. Geophys. Res.* (*Atmos*), **95,** 7617–7624

Troen, I. and Mahrt, L. 1986 A simple model of the atmospheric boundary layer; sensitivity to surface evaporation. *Boundary-Layer Meteorol.*, **37,** 129–148